The petrosal and bony labyrinth of extinct horses (Perissodactyla, Equidae) and their implications for perissodactyl evolution (#116824)

First revision

Guidance from your Editor

Please submit by **3 Oct 2025** for the benefit of the authors .

Structure and Criteria
Please read the 'Structure and Criteria' page for guidance.

Raw data check
Review the raw data.

Image check
Check that figures and images have not been inappropriately manipulated.

All review materials are strictly confidential. Uploading the manuscript to third-party tools such as Large Language Models is not allowed.
If this article is published your review will be made public. You can choose whether to sign your review. If uploading a PDF please remove any identifiable information (if you want to remain anonymous).

Files
Download and review all files from the materials page.

1 Tracked changes manuscript(s)
1 Rebuttal letter(s)
14 Figure file(s)
2 Table file(s)
1 Raw data file(s)
1 Other file(s)

Structure and Criteria

Structure your review

The review form is divided into 5 sections. Please consider these when composing your review:

- 1. Basic Reporting
- 2. Study design
- 3. Validity of the findings
- 4. General Comments
- 5. Confidential notes to the editor

- You can also annotate the review pdf and upload it as part of your review (optional).

You can also annotate this PDF and upload it as part of your review

When ready submit online.

Editorial Criteria

Use these criteria points to structure your review. The full detailed editorial criteria is on your guidance page.

Article types: Research and AI Application

BASIC REPORTING

Include the appropriate criteria template based on the type variable
Clear and unambiguous, professional English used throughout.

The article must be written in English and must use clear, unambiguous, technically correct text. The article must conform to professional standards of courtesy and expression.

Literature references, sufficient field background/context provided.

The article should include sufficient introduction and background to demonstrate how the work fits into the broader field of knowledge. Relevant prior literature should be appropriately referenced.

Professional article structure, figures, tables. Raw data shared.

The structure of the article should conform to an acceptable format of ‘standard sections’ (see our Instructions for Authors for our suggested format). Significant departures in structure should be made only if they significantly improve clarity or conform to a discipline-specific custom.

Figures should be relevant to the content of the article, of sufficient resolution, and appropriately described and labeled.

All appropriate raw data have been made available in accordance with our Data Sharing policy.

Self-contained with relevant results to hypotheses.

The submission should be ‘self-contained,’ should represent an appropriate ‘unit of publication’, and should include all results relevant to the hypothesis.

Coherent bodies of work should not be inappropriately subdivided merely to increase publication count.

EXPERIMENTAL DESIGN

Original primary research within Aims and Scope of the journal.
Research question well defined, relevant & meaningful. It is stated how research fills an identified knowledge gap.

The submission should clearly define the research question, which must be relevant and meaningful. The knowledge gap being investigated should be identified, and statements should be made as to how the study contributes to filling that gap.

Rigorous investigation performed to a high technical & ethical standard.

The investigation must have been conducted rigorously and to a high technical standard. The research must have been conducted in conformity with the prevailing ethical standards in the field.

Methods described with sufficient detail & information to replicate.

Methods should be described with sufficient information to be reproducible by another investigator.

VALIDITY OF THE FINDINGS

Impact and novelty not assessed. Meaningful replication encouraged where rationale & benefit to literature is clearly stated.

Decisions are not made based on any subjective determination of impact, degree of advance, novelty or being of interest to only a niche audience. We will also consider studies with null findings. Replication studies will be considered provided the rationale for the replication, and how it adds value to the literature, is clearly described. Please note that studies that are redundant or derivative of existing work will not be considered. Examples of "acceptable" replication may include software validation and verification, i.e. comparisons of performance, efficiency, accuracy or computational resource usage.

All underlying data have been provided; they are robust, statistically sound, & controlled.

The data on which the conclusions are based must be provided or made available in an acceptable discipline-specific repository. The data should be robust, statistically sound, and controlled.

Conclusions are well stated, linked to original research question & limited to supporting results.

The conclusions should be appropriately stated, should be connected to the original question investigated, and should be limited to those supported by the results. In particular, claims of a causative relationship should be supported by a well-controlled experimental intervention. Correlation is not causation.

Standout reviewing tips

The best reviewers use these techniques

Tip	*Example*
Support criticisms with evidence from the text or from other sources	*Smith et al (J of Methodology, 2005, V3, pp 123) have shown that the analysis you use in Lines 241-250 is not the most appropriate for this situation. Please explain why you used this method.*
Give specific suggestions on how to improve the manuscript	*Your introduction needs more detail. I suggest that you improve the description at lines 57- 86 to provide more justification for your study (specifically, you should expand upon the knowledge gap being filled).*
Comment on language and grammar issues	*The English language should be improved to ensure that an international audience can clearly understand your text. Some examples where the language could be improved include lines 23, 77, 121, 128 – the current phrasing makes comprehension difficult. I suggest you have a colleague who is proficient in English and familiar with the subject matter review your manuscript, or contact a professional editing service.*
Organize by importance of the issues, and number your points	*1. Your most important issue* *2. The next most important item* *3. …* *4. The least important points*
Please provide constructive criticism, and avoid personal opinions	*I thank you for providing the raw data, however your supplemental files need more descriptive metadata identifiers to be useful to future readers. Although your results are compelling, the data analysis should be improved in the following ways: AA, BB, CC*
Comment on strengths (as well as weaknesses) of the manuscript	*I commend the authors for their extensive data set, compiled over many years of detailed fieldwork. In addition, the manuscript is clearly written in professional, unambiguous language. If there is a weakness, it is in the statistical analysis (as I have noted above) which should be improved upon before Acceptance.*

The petrosal and bony labyrinth of extinct horses (Perissodactyla, Equidae) and their implications for perissodactyl evolution

Owen Axel Goodchild [1], **Sydney Nicole Rosen** [2], **Bastien Mennecart** [3], **Jin Meng** [4], **Jérémy Tissier** [Corresp. 4, 5]

[1] Richard Gilder Graduate School, American Museum of Natural History, New York, New York, United States

[2] Department of Biological Sciences, Vanderbilt University, Nashville, Tennessee, United States

[3] Naturhistorisches Museum Basel, Basel, Switzerland

[4] Department of Vertebrate Paleontology, American Museum of Natural History, New York, New York, United States

[5] Palaeobiosphere Evolution Unit, Royal Belgian Institute of Natural Sciences, Brussells, Belgium

Corresponding Author: Jérémy Tissier
Email address: jeremy.tissier123@gmail.com

Perissodactyla, or odd-toed ungulates, are represented today by 16 species of rhinoceroses, tapirs, and horses. Perissodactyls were much more diverse in the past, having a rich fossil record spanning from the earliest Eocene (~56 ma) to recent, including a myriad of extinct lineages. Despite over a century of study, the inter-relationships of some extinct perissodactyl families remain poorly resolved. New morphological characters are needed to help solve this issue. Recent studies suggest that the ear region, i.e., the petrosal and the bony labyrinth of the inner ear, is a valuable source of morphological characters for mammalian phylogenetic analyses. The petrosal is the bony structure protecting the inner ear, the organs of hearing and balance in mammals. However, perissodactyl petrosals are poorly documented and have not been used in such a phylogenetic frame. In this study, we describe the petrosals and inner ears of five European fossil equid taxa and perform a preliminary phylogenetic analysis. Despite its small sample size, our phylogenetic tree recovers important groupings, which suggests the petrosal is phylogenetically informative in equids. This study supports the relevance of the ear region for phylogeny and its potential to better resolve long-contentious relationships within Perissodactyla.

The petrosal and bony labyrinth of extinct horses (Perissodactyla, Equidae) and their implications for perissodactyl evolution.

Owen Axel Goodchild[1], Sydney Nicole Rosen[2], Bastien Mennecart[3], Jin Meng[4] & Jérémy Tissier[4,5]

[1] Richard Gilder Graduate School, American Museum of Natural History, New York, New York, USA
[2] Department of Biological Sciences, Vanderbilt University, Nashville, Tennessee, USA
[3] Naturhistorisches Museum Basel, Basel, Switzerland
[4] Department of Vertebrate Paleontology, American Museum of Natural History, New York, New York, USA
[5] Palaeobiosphere Evolution Unit, Royal Belgian Institute of Natural Sciences, Brussels, Belgium

Corresponding Author:
Jérémy Tissier
Rue Vautier 29, Brussels, 1000, Belgium
Email address: jeremy.tissier123@gmail.com

Abstract

Perissodactyla, or odd-toed ungulates, are represented today by 16 species of rhinoceroses, tapirs, and horses. Perissodactyls were much more diverse in the past, having a rich fossil record spanning from the earliest Eocene (~56 ma) to recent, including a myriad of extinct lineages. Despite over a century of study, the inter-relationships of some extinct perissodactyl families remain poorly resolved. New morphological characters are needed to help solve this issue. Recent studies suggest that the ear region, i.e., the petrosal and the bony labyrinth of the inner ear, is a valuable source of morphological characters for mammalian phylogenetic analyses. The petrosal is the bony structure protecting the inner ear, the organs of hearing and balance in mammals. However, perissodactyl petrosals are poorly documented and have not been used in such a phylogenetic frame. In this study, we describe the petrosals and inner ears of five European fossil equid taxa and perform a preliminary phylogenetic analysis. Despite its small sample size, our phylogenetic tree recovers important groupings, which suggests the petrosal is phylogenetically informative in equids. This study supports the relevance of the ear region for phylogeny and its potential to better resolve long-contentious relationships within Perissodactyla.

Introduction

Today, Perissodactyla Owen 1848, also known as odd-toed ungulates, are represented by 16 living species of rhinoceroses (n5), tapirs (n4), and horses (n7). Perissodactyls have a rich fossil history extending to the early Eocene ~56 million years ago (Ma; Bai, Wang & Meng, 2018). In addition to the ancestors of living perissodactyl groups, the perissodactyl fossil record contains several extinct families like the clawed Chalicotheriidae or bony-horned Brontotheriidae (Bai, Wang & Meng, 2018). Despite over a century of study, the interrelationships between extinct perissodactyl families and the relationships within those families remain controversial. Phylogenetic analyses using craniodental characters have longstanding issues, such as the internal relationships of Rhinocerotoidea (Tissier et al., 2018; Bai et al., 2020).

The discrepancies among these recent phylogenies highlight the necessity to investigate other structures of perissodactyl anatomy for new phylogenetically relevant characters. The petrosal is the paired basicranial bone housing the inner ear, which comprises the organs of balance (semicircular canals) and hearing (cochleae) in mammals (O'leary, 2010). The bony labyrinth is the inner bony surface of the petrosal bone, and is thus often considered as a good representation of the morphology of the inner ear. In many mammals other than perissodactyls, the petrosal and bony labyrinth are increasingly used in phylogenetic analyses and in understanding the paleobiology of these animals (Mennecart & Costeur, 2016; Mennecart et al., 2016; Aguirre-Fernández et al., 2017; Costeur et al., 2017; Costeur et al., 2018b; Costeur et al., 2018a; Aiglstorfer et al., 2017; Benoit et al., 2020; Mennecart et al., 2020; Evin et al., 2022; Wang et al.,

2022; Mennecart et al., 2022; Orliac et al., 2023; Zhang & Tong, 2024). The petrosal and bony labyrinth have historically been a challenge to study because the bony labyrinth is completely enclosed in the petrosal, while the petrosal is often enclosed in the skull. Computed Tomography (CT) allows for the visualization of internal and external details of the petrosal, and the generation of endocasts of the bony labyrinth within. The petrosal of perissodactyls is relatively poorly known and has yet to be used in large-scale phylogenetic analyses (see Mateus, 2018 for a review).

This study aims to describe the petrosal, bony labyrinth, and stapes (when preserved) of five different extinct equids, explore their morphological variations, and assess whether the petrosal characters presented by O'Leary (2010) and Mateus (2018) are phylogenetically informative in these taxa.

Materials & Methods

Taxonomy and specimens

This study involves seven petrosal specimens (Tab. 1; Fig. 1) from five European fossil equids housed in the collections of the Natural History Museum of Basel, Switzerland (NMB) that were previously identified in the collection. We confirmed the identification based on the reported taxonomic diversity from each locality, and by comparison with the petrosal of extant *Equus* (e.g. in O'Leary, 2010 and Danilo et al., 2015), as well as with Artiodactyla (O'Leary, 2010), *Tapirus* (O'Leary, 2010; Mateus, 2018) and *Ceratotherium* (Robert et al., 2021).We also had access to the petrosals of *Equus caballus* (AMNH FM 118) and *Tapirus terrestris* (AMNH FM 14103) described by O'Leary (2010) for comparison and phylogenetic analysis.

Anchitherium aurelianense Cuvier, 1825 is the oldest equid in our study (Agustí & Antón, 2002). The petrosal imaged here comes from the famous Middle Miocene locality of Sansan dated to the Astaracian European Land Mammal Age ~15 Ma (Alberdi, Ginsburg & Rodríguez, 2004). Its identification in our study remains tentative, as we could not directly compare it with another clearly identified specimen. *Hipparion* belongs to a large group of fossil equids, the Hipparionini, from across North America, Asia, Europe, and Africa (Bernor et al., 2021). The two *Hipparion* specimens in this study come from two different sites: Montredon (Vallesian, 11-9 Ma; France) and Concud (upper Turolian, ~5 Ma, Spain; Forstén, 1982). All the *Equus* material in our sample comes from the Early Pleistocene (Villafranchian), one from Valdarno (Italy) and three from Senèze (France). They belong to the stenonine lineage that consists of Early Pleistocene European and African *Equus* (Cirilli et al., 2021a). The specimen from Valdarno belongs to *Equus stenonis,* while the specimens from Senèze belong to *Equus senezensis* (Cirilli et al., 2021b).

Table 1.

Figure 1.

CT scans and segmentation

The equid material for this project was scanned at the Biomaterials Science Centre of the University of Basel, Switzerland, using a Phoenix Nanotom, GE. Tomograms were segmented using 3D Slicer (Fedorov et al., 2012) to extract the petrosal, the digital endocast of the bony labyrinth, and the stapes. 3D models representing seven petrosal bones, six bony labyrinths, and three stapes were generated in 3D Slicer. All tomograms and 3D models of petrosals, bony labyrinths, and stapes are available for download on Morphosource (temporary access link for peer-review: https://www.morphosource.org/projects/000720375/temporary_link/KB8T8eo9geShZZ6F4Cn6Tjz3?locale=en).

Measurements

Measurements were digitally taken using the "Measuring Tool" MeshLab2022.02 (Cignoni et al., 2008). We followed the linear measurement methods outlined in Ekdale (2013, figure 3), and measured the height and width of the cochlea used for the calculation of the aspect ratio and the height, width, and length of the semicircular canals used for the calculation of the radius of curvature (Tab. 2).

Table 2.

Character scores and phylogenetic analysis

We constructed a character matrix in Mesquite, combining characters from the petrosal and bony labyrinth, which is provided in Nexus format in Supplemental File 1. The list of characters and characters states is included in the matrix file, and detailed in Supplemental File 2. We scored the 3D models of the petrosal and stapes with characters from Spaulding et al. (2009; available in morphobank: http://dx.doi.org/10.7934/X188). We retained 33 characters which exclusively concern the petrosal bone, and the two characters of the stapes (characters 65 and 66 of Spaulding et al. 2009). We excluded characters from the auditory bulla, which was not preserved in our fossil specimens. We added 9 characters from Mateus (2018) for a total of 42 petrosal characters (see Supplemental File 2). We scored the 3D models of the bony labyrinth according to the 6 discrete characters of Ekdale (2013; available in morphobank: http://dx.doi.org/10.7934/X1905). We scored *Equus przewalskii* in the matrix based on the descriptions and figures of Danilo et al. (2015) and used the original scores of *Hyopsodus*, *Tapirus terrestris*, and *Equus caballus* from Spaulding et al. (2009) as well as those of *Equus* from the matrix of Ekdale (2013) and of *Hyopsodus* and *Tapirus terrestris* from Mateus (2018). In total, our matrix includes 50 characters (9 are parsimony informative in our analysis and 29 are constant) and 10 terminal taxa.

We performed a maximum parsimony (MP) analysis using PAUP4 (Swofford, 2002). Given the small number of taxa in our sample, we used the exhaustive search function to search all possible tree topologies to obtain the most parsimonious tree(s). *Hyopsodus* was set as outgroup and all characters are considered as unordered. The optimization settings were set on ACCTRAN.

We performed a Bootstrap analysis in PAUP4, using 100 replicates with a full heuristic search algorithm. For each boostrap replication, 1000 heuristic replicates were done, holding 100 trees at each step, with a TBR algorithm and a reconnection limit of 8.

Anatomical terminology

The anatomical terminology used for the description of the stapes follows Orliac and Billet (2016). The terminology used for the petrosal follows O'Leary (2010) and the terminology of the inner ear follows Ekdale (2013). More specifically, we follow the terminology of Robson and Theodor (2025) for the subarcuate depression of the petrosal (rather than fossa).

Biostratigraphy

The stratigraphical framework is based on the geological timescales and European Land Mammal Ages (ELMA) for the Neogene (Raffi et al. 2020).

Results

Systematic Paleontology

Mammalia, Linnaeus 1758

Perissodactyla, Owen 1848

Equidae, Gray 1821

Anchitheriinae, Leidy 1869

Anchitherium, Meyer 1844

Anchitherium aurelianense, Cuvier 1825

Material

An isolated right petrosal, NMB.San.15063

Locality and age

Sansan, Gers, France; Miocene, Astaracian (MN 6)

Description and comparison. The petrosal of *Anchitherium aurelianense* (NMB.San.15063; Fig. 2) is 2.11 cm long anteroposteriorly. The specimen is largely complete, with minor damage to the mastoid region. The bony labyrinth could not be segmented in this specimen due to the absence of contrast between the sediment infilling the bony labyrinth and the petrosal bone.

The petrosal of *A. aurelianense* is markedly different in several aspects from that of *Equus caballus* (O'Leary 2010). In anterior view (Fig. 2C), *A. aurelianense* lacks the endocranial projection of the superiormost aspect of the petrosal seen in *Equus*. The *crista interfenestralis* is broader and more rounded than in *E. caballus*. The epitympanic

wing is small, forming a low protrusion from the promontorium. The wing is rounded rather than pointed and does not protrude. The subarcuate depression is very shallow. The *hiatus Fallopii* is small and opens on the ventromedial border of the petrosal, close to the *tegmen tympani* (Fig. 2B).The stapedial muscle fossa is oval-shaped and located in the facial *sulcus*, below the *crista interfenestralis* separating the *fenestrae vestibuli* and *cochleae*. The *fenestra cochleae* is round, while the *fenestra vestibuli* is oval. *Anchitherium* possesses a notably smaller *tegmen tympani* than *Equus caballus* (O'Leary 2010). Unlike in *E. caballus*, the *tegmen tympani* is flattened and is not prominent in dorsolateral view (Fig. 2B). The surface of the *tegmen tympani* is smooth, forming an angled surface anteromedial to the mastoid region. The *tegmen tympani* lacks raised bumps and the *hiatus Fallopii* excavates a portion of its medial edge.

The dorsomedial surface of the petrosal in *A. aurelianense* is largely smooth, like *E. caballus* (O'Leary 2010), but with some rugosity along the anterior margin and along the floor of the grooove anterior to the internal acoustic meatus (Fig. 2D). Since this petrosal was found as an isolated element we interpret this rugosity as the result of taphonomic weathering. The crista transversa is a sinuous ridge of bone between the superior and inferior acoustic foramina, as in *E.caballus*, but is thicker. The cochlear aqueduct is small and slit-like (Fig. 2D-E). The vestibular aqueduct forms a round, open hole (Fig 2D).

The peculiar nature of the *tegmen tympani* in the petrosal of *Anchitherium* recalls the "uninflated" condition seen in the early diverging eutherians like *Protungulatum* (O'Leary 2010). As in *Protungulatum*, the *tegmen tympani* is flat in *Anchitherium*. The surface is moderately raised in dorsomedial view relative to the internal acoustic meatus, while in *Protungulatum* the *tegmen tympani* is flatter in dorsomedial view. The *tegmen tympani* morphology of *Anchitherium* is somewhat intermediate between the uninflated *tegmen tympani* of *Protungulatum* and the smaller but inflated *tegmen tympani* of *Hipparion*. It is puzzling then, that the literature reports the earlier diverging equid *Orohippus* as having an inflated *tegmen tympani* (Cifelli, 1982). Indeed, all the fossil tapirs Mateus (2018) referred to have an inflated *tegmen tympani*. See the discussion for further consideration.

A. aurelianense lacks an anterior process of the *tegmen tympani*. A ventrolateral tuberosity was present in *A. aurelianense* (Fig. 2A-C). Medial to the external acoustic meatus is a relatively deep epitympanic recess (Fig. 2A). *A. aurelianense* lacks a distinct stylomastoid notch.

The petrosal is narrow in ventromedial view (Fig. 2E), widening into a fan-shaped mastoid region like in *E. caballus* (O'Leary, 2010). The mastoid region is very incomplete. It was considered here to be large as per O'Leary 2010's definition but is notably smaller than that of *E. caballus*. The preserved element of the mastoid is consistent with a wedge shape as described in O'Leary (2010).

Figure 2.

Equinae, Steinmann and Döderlein 1890
Hipparionini, Quin 1955
Hipparion, Christol 1832
Hipparion depereti, Sondaar 1974

Material

An isolated left petrosal, NMB.A.Mo655

Locality and age

Montredon, France; Late Miocene Vallesian (MN 10).

Description and comparison. The Montredon *Hipparion*, *Hipparion depereti*, specimen NMB.A.Mo655, is a largely complete petrosal, with minor damage to the *tegmen tympani* and the mastoid region. Segmentation of its bony labyrinth was made challenging by the presence of very dense infilling (possibly iron). NMB.A.Mo.655 is an isolated petrosal measuring 3.9 cm in length. This petrosal is intermediate between *Anchitherium* and *Equus*. Notably, the petrosal of *H. depereti* is more massively constructed and broader than that of *Anchitherium aurelianense*. There are notable distinctions from *Equus*, however. The *promontorium* gives rise to the epitympanic wing (Fig. 3B), which is small and rounded rather than pointed as in *E. caballus* (O'Leary, 2010), but longer than in *Anchitherium*.

Between the epitympanic wing and the *tegmen tympani* lies the opening for the *hiatus Fallopii* (Fig. 3B), which is very small. The fossa for the *tensor tympani* is located between the *hiatus Fallopii* and the *fenestra vestibuli*. The *fenestra cochleae* is round, and the *fenestra vestibuli* is oval. The stapedial muscle fossa is deep and round in the facial sulcus, just below the crista interfenestralis. The stylomastoid notch is thin and rather shallow. The *tegmen tympani* (Fig. 3C, D) is more greatly inflated than in *A. aurelianense* but much less than in *E. caballus*. There is no anterior process of the *tegmen tympani*. In dorsomedial view (Fig. 3E), the surface of the area around the internal acoustic meatus is smooth. However, this specimen has been abraded, making the surface appear more rugose than in life. The subarcuate depression is wide and shallow, as in *E. caballus* (O'Leary, 2010) and the petromastoid canal is absent. In dorsolateral view (Fig. 3C), the petrosal is narrow anteriorly and expands into a fan-shaped mastoid region posteriorly. The medial surface of the petrosal is flat. The basicapsular groove can be seen along the dorsal margin of the petrosal (Fig. 3F). The cochlear aqueduct is a very small hole at the ventromedial margin (Fig. 3E-F), although located more ventrally than in *Tapirus terrestris* (like *E. caballus*). The vestibular aqueduct is visible but the mastoid part of the petrosal is broken. The ventral knob-like area is well-preserved, but lacking the dorsal point seen in *E. caballus* (O'Leary, 2010).

Figure 3.

The bony labyrinth of NMB.A.Mo.655 is more poorly preserved than the other specimens in this study, as dense infilling obscured its shape . Nevertheless, the gross morphology of the bony labyrinth can be described and discussed. It shows little post-mortem deformation. The bony labyrinth fills much of the volume of the petrosal, but not to the extent observed in *Hyopsodus lepidus* (Ravel & Orliac, 2015). The presence of a secondary bony lamina is unclear; due to poor preservation or a genuine absence. In the bony labyrinth of the earlier diverging equid *Xenicohippus osborni* no secondary bony lamina was observed, although deformation made that observation questionable (Ravel & Orliac, 2015). In the more derived *E. caballus*, the secondary bony lamina is weakly developed (Ekdale, 2013). The cochlear spiral aspect ratio (0.55) is higher than that of *E. caballus*,, although notably lower than that observed in *Hyopsodus lepidus* (Ravel & Orliac, 2015). The cochlea completes two and a half turns and is loosely coiled (Fig. 4B) like *E. caballus* (Ekdale, 2013). As in *X. osborni*, the cochlea is elliptical, with the anteroposterior axis longer than the mediolateral axis. The cochlear aqueduct is straight, narrowing as it nears its external aperture as in *E. caballus* (Ekdale, 2013), and short. The lateral semicircular canal widens anteriorly to form a lateral ampulla (Fig. 4A). Posteriorly, the lateral semicircular canal and posterior semicircular canal appear to form a secondary common crus (Fig. 4), unlike *E. caballus*, although this may be an artefact of poor resolution in the model. (Ekdale, 2013). Like both *X. osborni* and *E. caballus*, the arc of the anterior semicircular canal possesses the largest radius and the greatest height of the three (Ravel & Orliac, 2015). The lateral semicircular canal attaches more dorsally to the vestibule than the posterior semicircular canal. The angles between the posterior and lateral semi-circular canals, and between the anterior and lateral semi-circular canals lay at a right angle to one another (Fig. 4C).The angle between the posterior and anterior canal is slightly obtuse (Fig. 4D). The anterior and posterior canals are relatively rounded, while the lateral one is ovoid in shape. The long endolymphatic sac is triangular in shape and posteriorly projected. It starts high, almost at the dorsal end of the common crus, but this could also be due to the poor preservation of the specimen. There is no clear distinction between the fenestrae vestibuli and cochleae, due to the preservation of the specimen. The cochlea is not in contact with the vestibule.

Figure 4.

Hipparion concudense, Pirlot 1956

Material

An isolated left petrosal, NMB.Ccd.3

Locality and age

Concud 3, Teruel, Spain; Late Miocene, Turolian (MN 12).

Description and comparison. The Concud 3 *Hipparion*, *Hipparion concudense*, specimen is an almost entirely complete petrosal, with only minor damage to the mastoid region, measuring 3.15 cm in length. It preserved a stapes fallen within the bony labyrinth. The petrosal of *H. concudense* is similar in most aspects to its geologically older relative *H. depereti*. The epitympanic wing is a low-rounded structure protruding gently from the anterior portion of the promontorium. The caudal tympanic process, located posterior to the *fenestra cochlae*, is mediolaterally broad but not to the same extent observed in *E. caballus* (O'Leary, 2010). The mastoid region is large, occupying about half the bone. As in both extinct and extant equids, the mastoid is shaped as a knob. Likewise, as in the other fossil equids described here, the mastoid region is incomplete, leaving only the fan-like proximal portion of the mastoid. The mastoid of *H. concudense* is not as greatly expanded as that of *H. depereti*. The thin bony lamina that covers the *hiatus Fallopii* is still preserved and separates the secondary facial foramen from the anterior hole of the *hiatus Fallopii* (Fig. 5B). The stapedial muscle fossa is extremely deep, large and oval-shaped, although this may be related to allometry. The facial sulcus is deep.

In ventrolateral or tympanic view, the promontorium is smooth, with no sign of a sulcus for the stapedial artery (Fig. 5B). The promontorium has a slight bulge to accommodate the cochlea within, like *H. depereti* (Fig. 5C-F). The fenestra cochleae is similar in shape and relative size to that of *E. caballus* (O'Leary, 2010), oval shaped and smaller than the fenestra vestibuli. The *fenestra vestibuli* is more reniform than that of *H. depereti* (Fig. 3B; 5B). The crista interfenestralis is broader than *E. caballus*, but not as broad as *Anchitherium aurelianense* (Fig. 1A; 5B).

In dorsomedial view (Fig. 5E), the *tegmen tympani* is markedly smaller than *E. caballu*s, though slightly inflated laterally. The *tegmen tympani* has a flat surface and lacks the large anterior process seen on *E. caballus* (O'Leary, 2010). The basicapsular groove sits along the dorsal edge of the petrosal (Fig. 5D), and the cochlear aqueduct (Fig. 5E-F) sits in a slit situated more ventrally than ventromedially as in *E. caballus* (O'Leary, 2010). The vestibular aqueduct exits in a very similar position as in E. caballus on the dorsomedial face of the petrosal (Fig. 5E). In the anterior view (Fig. 5D), the superiormost portion of the petrosal does not project medially, at least not to the extent seen in *E. caballus* (O'Leary, 2010).

Figure 5.

The bony labyrinth of *Hipparion concudense* is better preserved than that of *H. depereti*. Like NMB.A.Mo.655, it shows little post-mortem deformation. A faint secondary bony lamina extends along the first 2/3rds of the basilar turn. The cochlea forms a loose spiral of 2.5 turns, like both *H. depereti* and *E. caballus* (Ekdale, 2013). The cochlear aqueduct narrows as it nears the aperture of the petrosal, as observed in

H. depereti. The anterior semicircular canal has both the greatest height and radius of curvature. Like *E. caballus,* the posterior entry of the lateral semicircular canal is through the posterior ampulla, and the lateral semicircular canal attaches more dorsally to the vestibule than the posterior semicircular canal. The lateral semicircular canal sits at a right angle relative to both the anterior and posterior semicircular canals. The angle between the posterior and anterior canal (Fig. 6D) is more obtuse than in *Hipparion depereti*. It also differs from *Hipparion depereti* by its more posteriorly elongated lateral canal in dorsal view (Fig. 6D). The anterior canal is more rounded than the posterior one. The lateral one is ovoid in shape rather than a semicircle. The long endolymphatic sac is triangular in shape and posteriorly projected. It starts below the common crus, and runs mostly parallel to it. There is an inflection between the vestibule and the cochlea. The cochlea is few detached (short distance between the start of the first turn and the start of the second turn) from the vestibule.

The stapes of *H. concudense* (Fig. 7A) was preserved inside the vestibule of the bony labyrinth, which happens occasionally, as reported by Orliac and Billet (2016). It seems to be broken or poorly preserved, lacking most of its medial side (Fig. 7A). The general shape is quite similar to that of *Equus caballus* illustrated by Doran (1878: pl. 61, fig. 3). In lateral view, the foramen intercrurale is large and rectangular. The *capitulum* cannot be distinguished from the rest of the body of the stapes or is not preserved. The *basis stapedis* is oval-shaped.

Figure 6.

Figure 7.

Equini Quinn 1955

Equus Linnaeus 1758

Equus stenonis Cocchi 1867

Material

An isolated left petrosal, NMB.V.A.2753

Locality and Age

Valdarno, Italy; Early Pleistocene, Villafranchian age (MNQ 18).

Description and comparison. *Equus stenonis* from Valdarno is represented by an isolated petrosal (NMB.V.A.2753) measuring 3.55 cm in length. The petrosal is well preserved, with the only major damage being to the mastoid region. The Valdarno *Equus* preserved a stapes within the bony labyrinth. In overall character, the petrosal is strikingly more similar to *E. caballus* (O'Leary, 2010) and *E. senezensis* than to *Hipparion* and especially *Anchitherium*. *E. stenonis* and *E. senezensis* are similar to *E. caballus* in possessing a prominent anterior process of the *tegmen tympani*, while *Hipparion* and *Anchitherium* have low tegmina tympani lacking such a pronounced anterior process. This anterior process ends in a point, as in *E. caballus* (O'Leary,

2010). The anterior process of the *tegmen tympani* of *Equus stenonis* does not extend anterior to the promontorium. The caudal tympanic process is wide and smooth (Fig. 8B), with an expansion similar to extant *E. caballus* rather than *Hipparion* or *Anchitherium*. The mastoid region is large, with a broad proximal area like the other equids in this study. The subarcuate depression is wide and shallow as in *E. caballus* (O'Leary, 2010). The vestibular aqueduct opens in a slit lateral to the subarcuate depression and posteromedial to the cochlear aqueduct. The mastoid meets and joins the caudal tympanic process such that the mastoid juts out at an angle when viewed in ventrolateral view (Fig. 8F). Two grooves along the ventromedial edge of the bone demarcate the basicapsular groove (Fig. 8 D-E), with the cochlear aqueduct laying at the posterior edge of this groove. The ventrolateral side (Fig. 8B) is not very well preserved, and the segmentation of this area was difficult due to the preservation of the bulla, which we excluded in the figures. The *hiatus Fallopii* is not well preserved but may lie between the epitympanic wing and the *tegmen tympani* (Fig. 8B). The facial *sulcus* is barely visible and quite shallow. The petrosal is narrow in ventromedial view, expanding into a fan-shaped mastoid process (Fig. 8F). The promontorium is barely distinguished but seems elongated and bordered by a long posteromedial flange. The *fenestrae vestibuli* and *cochleae* are similar-sized.

Figure 8.

The bony labyrinth of *Equus stenonis* is nearly identical to *E. caballus* (Ekdale, 2013). The cochlea is loosely coiled, forming 2.5 turns. The cochlea takes on an elliptical shape, longer anteroposteriorly than mediolaterally. A faint bony lamina extends along the first 2/3rds of the basilar turn of the cochlea (Fig. 9). Like *E. caballus* the posterior entry of the lateral semicircular canal is through the posterior ampulla (Fig. 9C), the largest semicircular arc radius of curvature is in the anterior semicircular canal, and the lateral semicircular canal attaches more dorsally to the vestibule than the posterior semicircular canal (Fig. 9C). The posterior ampulla is larger than in *Hipparion* (Fig. 9B-C). However, the anterior canal seems to be more elliptic than the posterior one due to a straight projection of the anterior canal when connecting with the common crus (Fig. 9B). The lateral canal is slightly ovoid in shape (Fig. 9D) and larger than in *H. concudense*. The small endolymphatic sac is triangular in shape and posteriorly projected, not in line with the common crus (Fig. 9B). It starts close to the base of the common crus due to a very short and posteriorly projected vestibular aqueduct (Fig. 9C). There is an inflection between the vestibule and the cochlea. The cochlea is few detached (short distance between the start of the first turn and the start of the second turn) from the vestibule (Fig. 9A). The cochlear vein is preserved (Fig. 9B-C), ventral to the cochlear aqueduct, as in *E. caballus* (Ekdale, 2013).

The stapes of *Equus stenonis* (Fig. 7B) is very similar to that of *H. concudense*, but it is more complete. The foramen *intercrurale* is larger on the lateral side than on the medial side, as observed in some artiodactyls (Orliac and Billet 2016). The *basis stapedis* is oval-shaped (Fig. 7B). In medial and lateral views (Fig. 7B), the stapes is roughly triangular. The *capitulum stapedis* cannot be differentiated from the rest of the body of the stapes. In medial view, the *foramen intercrurale* is much smaller than on the lateral side.

Figure 9.

Equus senezensis, Azzaroli 1964

Material

Three petrosals, including the left and right petrosals and one stapes of a single individual (NMB.Se.141) and an isolated right petrosal (NMB.Se.554).

Locality and Age

Senèze, France; Early Pleistocene, Villafranchian (MNQ 18).

Description & comparison. *Equus senezensis* was represented by three petrosals, two of which represent the left and right petrosals of a single individual NMB.Se.141, and one from NMB.Se.554. The petrosals vary in size from 3.60 to 3.94 cm anteroposteriorly. They differ from that of *Equus caballus* (O'Leary, 2010) in several ways. Between the *fenestra cochleae* and the *fenestra vestibuli* is a *crista interfenestralis* that is pronounced, but less distinct than in *E. caballus* (O'Leary, 2010). The fossa for the *tensor tympani* muscle is a large, oval, and deep depression (Fig. 10D). It significantly excavates the surrounding *tegmen tympani* (Fig. 10B). The epitympanic wing is present and protrudes from the *promontorium* but is very small (Fig. 10B). There is a distinct anterior hole for the *hiatus Fallopii* and it is relatively large (Fig. 10B). A posteromedial flange extends from the *promontorium* such that the *promontorium* is surrounded by a complete, flat flange of bone similar to that of *E. caballus* (O'Leary, 2010), though it appears to extend even further posteriorly. On the second specimen (NMB.Se.554), the fossa for the *tensor tympani* muscle is shallower, and oval (Fig. 11B). The *tegmen tympani* is flat and moderately inflated, contributing to about one-fifth the total width of the ventrolateral view though slightly more inflated than that of *E. caballus* (O'Leary, 2010). The anterior process of the *tegmen tympani* is larger than that of *E. caballus* and extends anterior to the promontorium before terminating in a less pronounced point (O'Leary, 2010). The mastoid region is large and wedge-shaped, irregular, and knobby, though it appears rounder than that of *E. caballus* (O'Leary, 2010). The facial sulcus and stapedial muscle fossa cannot be observed.

The ventromedial edge of the bone has a basicapsular groove, and at its posterior edge houses a small cochlear aqueduct (Fig. 11E). The slit for the cochlear aqueduct is smaller in NMB.Se.554 (Fig. 11E) than in NMB.Se.141 (Fig. 10E). The

vestibular aqueduct opens in a slit lateral to the subarcuate depression and posteromedial to the cochlear aqueduct (Fig. 10E, 11E). In the ventromedial view, the petrosal is narrow and widens into a fan-shaped mastoid region with bumps and projections. The ventromedial surface is relatively flat (Fig. 11C). There are vascular grooves on the dorsolateral side of the *tegmen tympani* (Fig. 10C). The cochlear aqueduct is a small hole at the ventromedial margin but is found within a large slit (Fig. 10D-E).

We can observe patterns of intra-individual variation due to asymmetry in the petrosal of *Equus senezensis*. The two petrosals of NMB.Se.141 differ indeed in some respects, such as the subarcuate depression, which is smaller in the right petrosal than in the left one (see additional specimen available on Morphosource project: https://www.morphosource.org/projects/000720375/temporary_link/KB8T8eo9geShZZ6F4Cn6Tjz3?locale=en). Such variation is consistent with Danilo et al (2015)'s study of modern *Equus,* where the size, morphology, elongation, and depth of the subarcuate depressioncan be highly variable among individuals.

Figure 10.

Figure 11.

The basal portion of the cochlear coil of *Equus senezensis* (NMB.Se.141 and NMB.Se.554; Fig. 12-13) begins slightly straight before forming a pronounced curve that becomes the spiral shape of the cochlea separating the cochlea from the vestibule. The latter part of the coil begins as a loose spiral that becomes tighter towards the apex. The coil remains tightly wound consistently after about the first quarter of the first basal turn. The cochlea completes about 2.5 turns (Fig. 12A, 13A) and is more tightly coiled than *Equus caballus* (Ekdale, 2013). The cochlea of *Equus senezensis* has an aspect ratio ranging from low (0.44) to high (0.58; Tab. 2.) in contrast to the low aspect ratio of *E. caballus* (0.41; Ekdale 2013, tab. 2). There is no secondary bony lamina on the cochlea of either the left or right bony labyrinth of NMB.Se.141 (Fig12A. 13A), but NMB.Se.554 does preserve a faint secondary bony lamina like *E. stenonis,* and *E. caballus* (Ekdale, 2013).

NMB.Se.554 has the spherical and elliptical recesses separated by a narrowing of the vestibule. This condition is observed in both *E. caballus* (Ekdale, 2013) and *E. senezensis* but is more pronounced in this individual than in NMB.Se.141. The entry of the lateral semicircular canal into the posterior one is through the posterior ampulla (Fig. 12B, 13B). The bony ring is quite pronounced and nearly parallel to the plane of the lateral semicircular canal. The posterior canal seems to be more elliptic than the anterior one.. The lateral one is relatively rounded (Fig. 12D, 13D). The large endolymphatic sac is rectangular in shape and posteriorly projected, not in line with the common crus (Fig. 12B, 13B). It starts almost at mid-height of the common crus due to

a slightly posteriorly projected vestibular aqueduct. There is an inflection between the vestibuleand the cochlea. The cochlea is few detached (short distance between the start of the first turn and the start of the second turn) from the vestibule.

Figure 12.

Figure 13.

The stapes of *Equus senezensis* was preserved inside the vestibule of the left petrosal NMB.Se.141 (Fig. 7C). It is overall quite similar to *Equus caballus* (Doran 1878), or the other two stapes described here, but is not well preserved. The *processus muscularis stapedis* is difficult to identify, but seems to be visible on the posterolateral face of the stapes (Fig. 7C). As in the other species, the *foramen intercrurale* is smaller on the medial side than on the lateral side. The *capitulum* cannot be identified.

Preliminary Phylogenetic Analysis

Using our combined dataset (see Material and Methods), we obtained 11 most-parsimonious trees of 24 steps, with a consistency index (CI) of 0.88, a retention index (RI) of 0.80, and a homoplasy index (HI) of 0.13. These 11 trees are included in the nexus file provided in Supplemental File 1. The strict consensus tree is shown in Fig. 14. Of the 50 characters in the analysis, 29 are constant and only 9 are parsimony informative. The clade Equidae is supported by six synapomorphies in ACCTRAN optimization:

- the absence of anterior process of the *tegmen tympani*,
- the apex of the anterior process of the *tegmen tympani* is large (when it is present)
- the apex of the anterior process of the *tegmen tympani* pointed (when it is present),
- the ventrolateral tuberosity of petrosal is present
- the lateral semicircular canal attaches more dorsally to the vestibule than the posterior canal,
- and the cochlear aqueduct is on the ventral face of the petrosal.

The clade Equinae is supported by three synapomorphies:

- the pars cochlearis protrudes ventromedially,
- the caudal tympanic process long,
- and the subarcuate depression wide.

Anchitherium has two autapomorphies, whereas *Equus stenonis* has one. *Equus* is monophyletic and supported by one unambiguous synapomorphy: the presence of an anterior process of the *tegmen tympani* (character 11). All perissodactyls, including *Tapirus*, differ from *Hyopsodus* by eight characters (characters 3, 20, 24, 25, 27, 29, 43

and 50).. In our analysis, *Hipparion* is paraphyletic, and *H. concudense* differs from *H. depereti* by the absence of extension of the fossa for the *tensor tympani* muscle.

Figure 14.

Discussion

Among both extant tapirs and horses, characters of the petrosal have been observed to be variable among individuals. Among equids, Danilo et al. (2015) described the variability of 14 petrosals of *Equus przewalskii* belonging to individuals of varying ages, sexes, and sizes (Danilo et al., 2015) while Costeur et al. (2017) also observed this variability in an ontogenetic series of *Bos*. They showed that the depth of the petrosal groove, the shape of the internal acoustic meatus, as well as the shape, size, and elongation of the subarcuate depression were individually variable depending on the age of the individual. Mateus (2018) showed that in *Tapirus terrestris* the depth and size of the subarcuate depression as well as the position of the caudal tympanic process and the *hiatus Fallopii*, are individually variable as in *E. przewalskii*. The subarcuate depression accounted for three characters in Spaulding et al., (2009) and one in Mateus (2018). All the perissodactyls in our analysis shared a shallow subarcuate depression. *Tapirus terrestris* and *Anchitherium aurelianense* were both scored as small for the size of the subarcuate depression while all the other perissodactyl taxa were scored as large.

We have to keep in mind that the petrosal bone, contrary to the bony labyrinth, is a structure that ossifies in parallel to the surrounding skull bones (Mennecart & Costeur 2016, Costeur et al. 2017). Because of this, this bone may greatly suffer from allometry (ontogenic and evolutionary) complexifying the interpretation of the evolutionary polarity of the characters.The bony labyrinth is an organ that fully ossifies during fetus stages in placental mammals (e.g. Mennecart & Costeur 2016, Costeur et al. 2017). Shape and size remain similar during the life of the animal, providing reliable results considering micro-and macroevolutionary processes (Evin et al. 2022, Mennecart et al. 2022). This organ may represent a structure with a neutral evolution in artiodactyls (Mennecart et al. 2022), where gradual changes can be observed.

The ear region of extinct perissodactyls remains poorly understood, relative to artiodactyls. The petrosal of extinct perissodactyls was only described for three equoids (Kits, 1956; Cifelli, 1982; O'Leary 2010), four tapiromorphs (Savage, et al., 1965; Radinsky & Expeditions (1921-1930), 1965; Colbert, 2006; Li and Wang, 2010; O'Leary, 2010), one brontothere (Mader, 2009), and one ancylopod (Bai, Wang & Meng, 2010) so far. The petrosal of rhinocerotoids is especially poorly understood. O'Leary (2010) briefly described the incomplete petrosal of *Dicerorhinus sumatrensis* in their morphological characters matrix, while Robert et al. (2021) investigated the petrosal and

bony labyrinth of *Ceratotherium simum simum*, and Manning (1985) reported an isolated petrosal of *Metamynodon*.

Moreover, recent molecular investigations have suggested that the extinct South American Native Ungulates (SANUs) were related to perissodactyls (Welker et al., 2015) but comparisons between the petrosals of SANUs and other placentals have been limited thus far, and have not included perissodactyls (Billet & Muizon, 2013). The contribution of the ear region into the phylogeny of perissodactyls may, therefore, also be key to illuminating their potential relationships to SANUs and other extinct hoofed mammal groups like phenacodontids and cambaytheres.

Conclusions

The result of our preliminary phylogenetic analysis suggests that the ear region is informative for perissodactyl phylogeny and invites future research. This limited analysis suggests that the petrosal morphology may be informative in family and genus-level cladistics, but it currently lacks precision for detecting generic level distinctions considering its inability to recover the monophyly of the genus *Hipparion*. Yet, it is also possible that the two species *H. depereti* and *H. concudense* do not belong to the same genus, since *Hipparion* may actually be paraphyletic according to another phylogenetic analysis (Sun et al. 2025). Further investigation is necessary to better understand the phylogenetic utility of the selected character in regards to their allometric constrains and variation. Moreover, the bony labyrinth has been proven to be a structure that evolves mostly neutrally in ruminants. Including more bony labyrinth characters, may be usefull for a better understanding of the perissodactyls' evolutionary history and to obtain more refined results. Obviously, a much larger sampling would be needed to fully investigate the phylogeny of Equidae or other perissodactyls, but we believe that the petrosal and inner ear's morphology could be a valuable addition in future larger-scale phylogenetic analysis. Although only ten characters were parsimony informative, we think that with a more diverse taxonomic sample, more characters would become phylogenetically informative.

Acknowledgements

This study would not have been possible without the support of Loïc Costeur (Natural History Museum of Basel), and we are thus highly indebted to him for providing access to the specimens studied here and for allowing us to CT-scan them. We are also extremely grateful to Georg Schulz (Department of Biomedical Engineering, University of Basel) for CT-scanning the specimens for us. The authors would like to thank Alana Gishlick and Ruth O'Leary (American Museum of Natural History) for access to and curation of some comparison specimens in this study. Additionally, we would like to thank R. Benjamin Sulser, John J. Flynn, Jocelyn A. Sessa, Bryce E. Koester, Jason P.

Downs, and Edward “Ted” B. Daeschler for useful interactions with the authors that helped this project develop. We gratefully acknowledge Eric G. Ekdale and Selina Viktor Robson for their comments, which greatly improved our manuscript, and the editor Blanca Moncunill-Solé for her work.

References

Aguirre-Fernández G, Mennecart B, Sánchez-Villagra MR, Sánchez R, Costeur L. 2017. A dolphin fossil ear bone from the northern Neotropics–insights into habitat transitions in iniid evolution. *Journal of Vertebrate Paleontology* 37:e1315817. DOI: 10.1080/02724634.2017.1315817.

Agustí J, Antón M. 2002. *Mammoths, sabertooths, and hominids: 65 million years of mammalian evolution in Europe*. New York: Columbia University Press.

Aiglstorfer M, Costeur L, Mennecart B, Heizmann EPJ. 2017. *Micromeryx? eiselei*—A new moschid species from Steinheim am Albuch, Germany, and the first comprehensive description of moschid cranial material from the Miocene of Central Europe. *PLOS ONE* 12:e0185679. DOI: 10.1371/journal.pone.0185679.

Alberdi MT, Ginsburg L, Rodríguez J. 2004. *Anchitherium aurelianense* (Mammalia, Equidae) (Cuvier, 1825) dans l’Orléanien (Miocène) de France.

Bai B, Meng J, Zhang C, Gong Y-X, Wang Y-Q. 2020. The origin of Rhinocerotoidea and phylogeny of Ceratomorpha (Mammalia, Perissodactyla). *Communications Biology* 3:1–16. DOI: 10.1038/s42003-020-01205-8.

Bai B, Wang Y, Meng J. 2010. New Craniodental Materials of *Litolophus gobiensis* (Perissodactyla, “Eomoropidae”) from Inner Mongolia, China, and Phylogenetic Analyses of Eocene Chalicotheres. *American Museum Novitates* 2010:1–27. DOI: 10.1206/678.1.

Bai B, Wang Y-Q, Meng J. 2018. The divergence and dispersal of early perissodactyls as evidenced by early Eocene equids from Asia. *Communications Biology* 1:1–10. DOI: 10.1038/s42003-018-0116-5.

Benoit J, Legendre LJ, Farke AA, Neenan JM, Mennecart B, Costeur L, Merigeaud S, Manger PR. 2020. A test of the lateral semicircular canal correlation to head posture, diet and other biological traits in “ungulate” mammals. *Scientific Reports* 10:19602. DOI: 10.1038/s41598-020-76757-0.

Bernor RL, Kaya F, Kaakinen A, Saarinen J, Fortelius M. 2021. Old world hipparion evolution, biogeography, climatology and ecology. *Earth-Science Reviews* 221:103784. DOI: 10.1016/j.earscirev.2021.103784.

Billet G, Muizon CD. 2013. External and internal anatomy of a petrosal from the late Paleocene of Itaboraí, Brazil, referred to Notoungulata (Placentalia). *Journal of Vertebrate Paleontology* 33:455–469. DOI: 10.1080/02724634.2013.722153.

Cifelli RL. 1982. The Petrosal Structure of *Hyopsodus* with Respect to That of Some Other Ungulates, and Its Phylogenetic Implications. *Journal of Paleontology* 56:795–805.

Cignoni P, Callieri M, Corsini M, Dellepiane M, Ganovelli F, Ranzuglia G. 2008. MeshLab: an Open-Source Mesh Processing Tool.

Cirilli O, Pandolfi L, Rook L, Bernor RL. 2021a. Evolution of Old World *Equus* and origin of the zebra-ass clade. *Scientific Reports* 11:10156. DOI: 10.1038/s41598-021-89440-9.

Cirilli O, Saarinen J, Pandolfi L, Rook L, Bernor RL. 2021b. An updated review on *Equus stenonis* (Mammalia, Perissodactyla): New implications for the European

679 early Pleistocene *Equus* taxonomy and paleoecology, and remarks on the Old
680 World *Equus* evolution. *Quaternary Science Reviews* 269:107155. DOI:
681 10.1016/j.quascirev.2021.107155.
682 Colbert MW. 2006. *Hesperaletes* (Mammalia: Perissodactyla), a new tapiroid from the
683 middle Eocene of southern California. *Journal of Vertebrate Paleontology* 26:697–
684 711. DOI: 10.1671/0272-4634(2006)26[697:HMPANT]2.0.CO;2.
685 Costeur L, Andrea V, Célia B, Mennecart B. 2018a. On some ruminant petrosal bones
686 and their bony labyrinth from Senèze (Villafranchian, France). *Revue de*
687 *Paleobiologie* 37:443–456. DOI: 10.5281/zenodo.2545101.
688 Costeur L, Grohé C, Aguirre-Fernández G, Ekdale E, Schulz G, Müller B, Mennecart B.
689 2018b. The bony labyrinth of toothed whales reflects both phylogeny and habitat
690 preferences. *Scientific Reports* 8:7841. DOI: 10.1038/s41598-018-26094-0.
691 Costeur L, Mennecart B, Müller B, Schulz G. 2017. Prenatal growth stages show the
692 development of the ruminant bony labyrinth and petrosal bone. *Journal of Anatomy*
693 230:347–353. DOI: 10.1111/joa.12549.
694 Danilo L, Remy J, Vianey-Liaud M, Mérigeaud S, Lihoreau F. 2015. Intraspecific
695 Variation of Endocranial Structures in Extant Equus: A Prelude to Endocranial
696 Studies in Fossil Equoids. *Journal of Mammalian Evolution* 22:561–582. DOI:
697 10.1007/s10914-015-9293-x.
698 Doran, A. H. 1878. XVIII. Morphology of the mammalian Ossicula auditûs. *Transactions*
699 *of the Linnean Society of London. 2nd Series. Zoology*, *1*(7), 371-497.
700 Ekdale EG. 2013. Comparative Anatomy of the Bony Labyrinth (Inner Ear) of Placental
701 Mammals. *PLOS ONE* 8:e66624. DOI: 10.1371/journal.pone.0066624.

Evin A, David L, Souron A, Mennecart B, Orliac M, Lebrun R. 2022. Size and shape of the semicircular canal of the inner ear: A new marker of pig domestication? *Journal of Experimental Zoology Part B: Molecular and Developmental Evolution* 338:552–560. DOI: 10.1002/jez.b.23127.

Fedorov A, Beichel R, Kalpathy-Cramer J, Finet J, Fillion-Robin J-C, Pujol S, Bauer C, Jennings D, Fennessy F, Sonka M, Buatti J, Aylward S, Miller JV, Pieper S, Kikinis R. 2012. 3D Slicer as an image computing platform for the Quantitative Imaging Network. *Magnetic Resonance Imaging* 30:1323–1341. DOI: 10.1016/j.mri.2012.05.001.

Forstén A. 1982. *Hipparion primigenium melendezi* Alberdi reconsidered. *Annales Zoologici Fennici* 19:109–113.

Kitts D. 1956. American *Hyracotherium* (Perissodactyla, Equidae). *Bulletin of the American Museum of Natural History* 110.

Mader BJ. 2009. Details of the cranial anatomy of a primitive diplacodont brontothere, cf. *Protitanotherium*, from the Wiggins Formation of Wyoming (Mammalia, Perissodactyla, Brontotheriidae). *Journal of Vertebrate Paleontology* 29:1224–1232. DOI: 10.1671/039.029.0414.

Manning, E. M. 1997. An early Oligocene rhinoceros jaw from the marine Byram Formation of Mississippi. *Mississippi Geology*, *18*(2)..

Mateus, A. L. D. 2018. The anatomical description of the osseous inner ear of tapirus and the evolution of the petrosal in perissodactyla. Ph.D. dissertation, Minas Gerais: Universidade Federal de Minas Gerais.

Mennecart B, Dziomber L, Aiglstorfer M, Bibi F, DeMiguel D, Fujita M, Kubo MO, Laurens F, Meng J, Métais G, Müller B, Ríos M, Rössner GE, Sánchez IM, Schulz G, Wang S, Costeur L. 2022. Ruminant inner ear shape records 35 million years of neutral evolution. *Nature Communications* 13:7222. DOI: 10.1038/s41467-022-34656-0.

Mennecart B, Guignard C, Dziomber L, Schulz G, Müller B, Costeur L. 2020. Allometric and Phylogenetic Aspects of Stapes Morphology in Ruminantia (Mammalia, Artiodactyla). *Frontiers in Earth Science* 8. DOI: 10.3389/feart.2020.00176.

Mennecart B, Rössner GE, Métais G, DeMiguel D, Schulz G, Müller B, Costeur L. 2016. The petrosal bone and bony labyrinth of early to middle Miocene European deer (Mammalia, Cervidae) reveal their phylogeny. *Journal of Morphology* 277:1329–1338. DOI: 10.1002/jmor.20579.

O'leary MA. 2010. An Anatomical and Phylogenetic Study of the Osteology of the Petrosal of Extant and Extinct Artiodactylans (Mammalia) and Relatives. *Bulletin of the American Museum of Natural History* 2010:1–206. DOI: 10.1206/335.1.

Orliac MJ, Maugoust J, Balcarcel A, Gilissen E. 2023. Paleoneurology of Artiodactyla, an Overview of the Evolution of the Artiodactyl Brain. In: Dozo MT, Paulina-Carabajal A, Macrini TE, Walsh S eds. *Paleoneurology of Amniotes : New Directions in the Study of Fossil Endocasts*. Cham: Springer International Publishing, 507–555. DOI: 10.1007/978-3-031-13983-3_13.

Radinsky LB. 1965. Early Tertiary Tapiroidea of Asia. *Bulletin of the American Museum of Natural History* 129:2.

748 Raffi, I., Wade, B. S., Pälike, H., Beu, A. G., Cooper, R., Crundwell, M. P., ... &
749 Vernyhorova, Y. V. 2020. The Neogene period. In *Geologic time scale 2020* (pp.
750 1141-1215). Elsevier.
751 Ravel A, Orliac MJ. 2015. The inner ear morphology of the 'condylarthran' *Hyopsodus*
752 *lepidus*. *Historical Biology* 27:957–969. DOI: 10.1080/08912963.2014.915823.
753 Robert MP, Carstens A, de Beer FC, Hoffman JW, Steenkamp G. 2021. Micro-anatomy
754 of the ear of the southern white rhinoceros (*Ceratotherium simum simum*).
755 *Anatomia, Histologia, Embryologia* 50:316–323. DOI: 10.1111/ahe.12632.
756 Robson SV, Theodor JM. 2025. Is *Bunomeryx* (Artiodactyla, Homacodontidae) an early
757 tylopod? A re-evaluation of evidence from the otic region, and a clarification of
758 some key anatomical terms. *Journal of Vertebrate Paleontology*, e2443094. DOI:
759 10.1080/02724634.2024.2443094
760 Spaulding M, O'Leary MA, Gatesy J. 2009. Relationships of Cetacea (Artiodactyla)
761 Among Mammals: Increased Taxon Sampling Alters Interpretations of Key Fossils
762 and Character Evolution. *PLOS ONE* 4:e7062. DOI:
763 10.1371/journal.pone.0007062.
764 Sun, BY., Liu, Y., Wang, SQ, & Deng, T. 2025. Occurrence of "*Hippotherium*" in the Old
765 World: a revision of two hipparion species in Eurasia. *Vertebrata PalAsiatica* 1: 57-
766 80. DOI: 10.19615/j.cnki.2096-9899.241120
767 Swofford D. 2002. PAUP* 4.0 : Phylogenetic Analysis Using Parsimony
768 Tissier, J., Becker, D., Codrea, V., Costeur, L., Fărcaş, C., Solomon, A., Venczel, M., &
769 Maridet, O. (2018). New data on Amynodontidae (Mammalia, Perissodactyla) from

770 Eastern Europe: Phylogenetic and palaeobiogeographic implications around the
771 Eocene-Oligocene transition. *PLoS One*, *13*(4), e0193774.
772 Wang S-Q, Ye J, Meng J, Li C, Costeur L, Mennecart B, Zhang C, Zhang J, Aiglstorfer
773 M, Wang Y, Wu Y, Wu W-Y, Deng T. 2022. Sexual selection promotes giraffoid
774 head-neck evolution and ecological adaptation. *Science* 376:eabl8316. DOI:
775 10.1126/science.abl8316.
776 Welker, F., Collins, M. J., Thomas, J. A., Wadsley, M., Brace, S., Cappellini, E., ... &
777 MacPhee, R. D. 2015. Ancient proteins resolve the evolutionary history of Darwin's
778 South American ungulates. *Nature*, *522*(7554), 81-84.
779 Zhang B, Tong H. 2024. The comparative anatomy of the petrosal bone and bony
780 labyrinth of four small-sized deer. *The Anatomical Record* 307:566–580. DOI:
781 10.1002/ar.25303.

Table 1(on next page)

Petrosal specimens examined in the study

Specimen and taxon	Locality	Age	Left or right	Bony Labyrinth	Stapes	Image dimensions	Inter-slice spacing (mm)
NMB.San.15063 *Anchitherium aurelianense*	Sansan, Gers France	Astaracian (MN 6)	Right	No (no contrast)	No	397x519x311	0.055x 0.055x 0.055
NMB.A.Mo.655 *Hipparion depereti*	Montredon, Occitanie, France	Vallesian (MN 10)	Left	Yes	No	672x729x600	0.056249x 0.056249x 0.056250
NMB.Ccd.3 *Hipparion concudense*	Concud 3, Teruel, Spain	Turolian (MN 12)	Left	Yes	Yes	410x656x530	0.056249x 0.056249x 0.056250
NMB.V.A.2753 *Equus stenonis*	Valdarno, Tuscany, Italy	Villafranchian (MN17)	Left	Yes	Yes	865x877x751	0.05625x 0.05625x 0.05625
NMB.Se.141 *Equus senezensis*	Senèze, Alpes-de-Haute-Provence, France	Villafranchian (MN 17)	Left	Yes	Yes	594x707x623	0.056249x 0.056249x 0.056250
NMB.Se.141 *Equus senezensis*	Senèze, Alpes-de-Haute-Provence, France	Villafranchian (MN 17)	~~Right~~Left	Yes	No	583x893x561	0.056249x 0.056249x 0.056250
NMB.Se.554 *Equus senezensis*	Senèze, Alpes-de-Haute-Provence, France	Villafranchian (MN 17)	~~Left~~Right	Yes	No	714x694x699	0.055x 0.055x 0.055

Table 1. Petrosal specimens examined in the study.

Table 2(on next page)

Bony labyrinth measurements of fossil equids

1 Table 2. Bony labyrinth measurements of fossil equids

Specimen #	Taxon	Source	ASC H/W aspect ratio	PSC H/W aspect ratio	LSC H/W aspect ratio	Number of cochlear turns	Cochlea aspect ratio
AMNH FM 55267	*Xenicohippus osborni*	Ravel & Orliac, 2015	1.00	0.98	1.13	_	_
NMB.A.Mo.655	*Hipparion depereti*	This study	1.13	1.25	0.83	2.5	0.55
NMB.Ccd.3	*Hipparion concudense*	This study	0.99	1.12	0.97	2.5	0.5
NMB.V.A.2753	*Equus stenonis*	This study	1.17	1.13	1.01	2.5	0.56
NMB-Se-554	*Equus senezensis*	This study	0.87	0.89	0.97	2.5	0.44
NMB-Se-141(left)	*Equus senezensis*	This study	1.05	1.09	1.05	2.5	0.58
NMB-Se-141(right)	*Equus senezensis*	This study	1.01	0.98	1.12	2.5	0.51
TMM-M-171	*Equus caballus*	Ekdale 2013	0.93	1.15	1.04	2.5	0.41

2

Figure 1

Map of fossil sites for equid specimens in this study (right) and the corresponding stratigraphic and biostratigraphic ages of those sites (left).

ELMMZ= European Large Mammal Mega-Zone, MNQ= Mammal Neogene/Quaternary Biostratigraphic Stage. Silhouettes from Phylopic made by Julian Bayona.

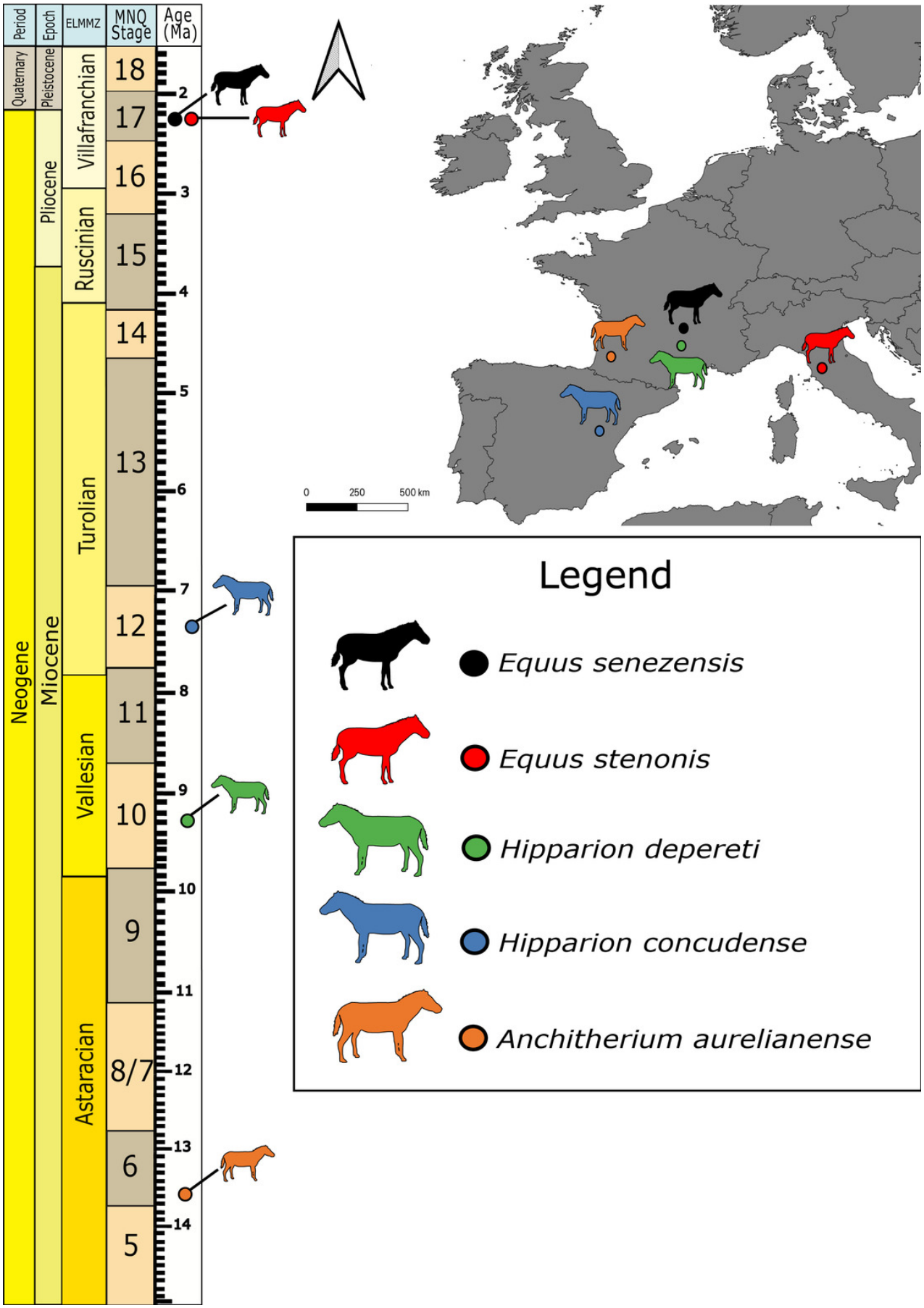
Period
Epoch
ELMMZ
MNQ Stage
Age (Ma)
Quaternary
Pleistocene
Villafranchian
18
17
16
Pliocene
Ruscinian
15
14
Neogene
Miocene
Turolian
13
12
Vallesian
11
10
9
Astaracian
8/7
6
5
2
3
4
5
6
7
8
9
10
11
12
13
14
0
250
500 km
Legend
Equus senezensis
Equus stenonis
Hipparion depereti
Hipparion concudense
Anchitherium aurelianense

Figure 2

Right petrosal (NMB.San.15063) of *Anchitherium aurelianense* from Sansan (mirrored).

(A) Ventrolateral view. (B) Ventromedial view. (C) Anterior view. (D) dorsomedial view. (E) Dorsolateral view. *Ant* = anterior, *dor.* = dorsal, *lat.* = lateral, *med.* = medial, *vent.* = ventral.

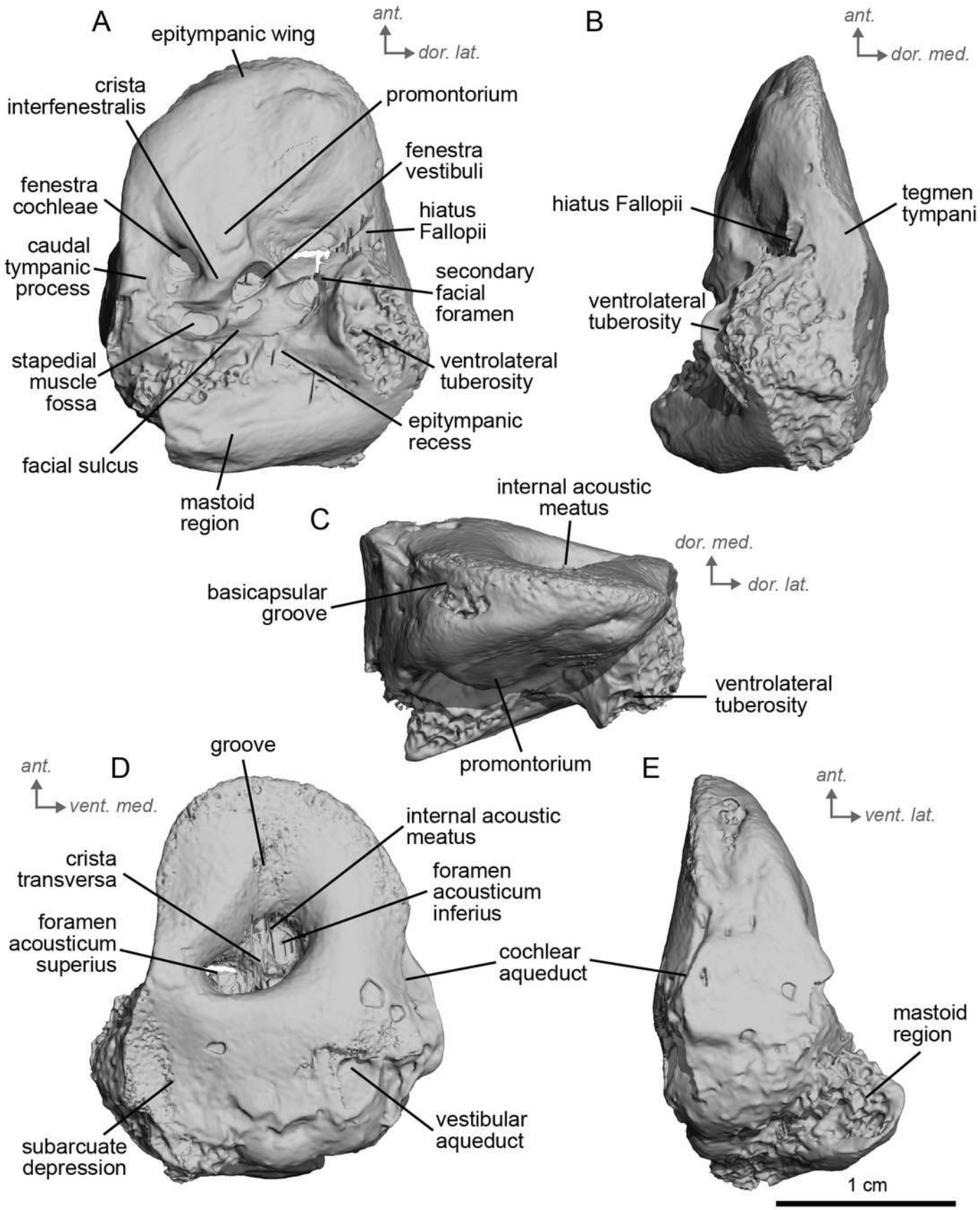
A
ant.
dor. lat.
epitympanic wing
crista interfenestralis
promontorium
fenestra vestibuli
fenestra cochleae
hiatus Fallopii
caudal tympanic process
secondary facial foramen
stapedial muscle fossa
ventrolateral tuberosity
epitympanic recess
facial sulcus
mastoid region
B
ant.
dor. med.
hiatus Fallopii
tegmen tympani
ventrolateral tuberosity
C
internal acoustic meatus
dor. med.
dor. lat.
basicapsular groove
ventrolateral tuberosity
promontorium
D
ant.
vent. med.
groove
internal acoustic meatus
crista transversa
foramen acousticum inferius
foramen acousticum superius
cochlear aqueduct
vestibular aqueduct
subarcuate depression
E
ant.
vent. lat.
mastoid region
1 cm

Figure 3

Left petrosal (NMB.A.Mo.655) of *Hipparion depereti* from Montredon.

(A) Ventrolateral transparent view. (B) Ventrolateral opaque view. (C) dorsolateral view. (D) Anterior view. (E) Dorsomedial view. (F) Ventromedial view. *Ant* = anterior, *dor.* = dorsal, *lat.* = lateral, *med.* = medial, *vent.* = ventral.

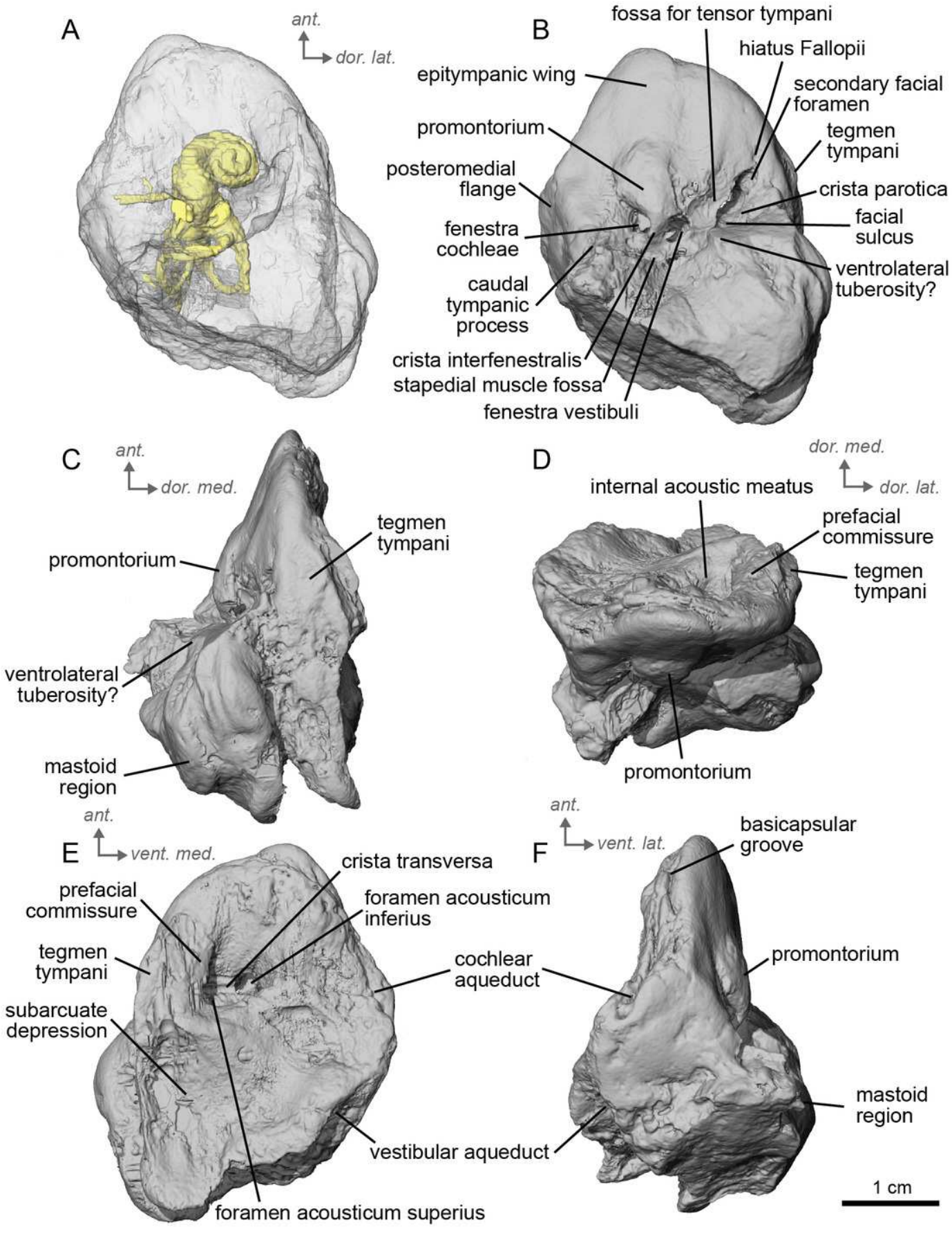
A
ant.
dor. lat.
B
fossa for tensor tympani
hiatus Fallopii
epitympanic wing
secondary facial foramen
promontorium
tegmen tympani
posteromedial flange
crista parotica
fenestra cochleae
facial sulcus
ventrolateral tuberosity?
caudal tympanic process
crista interfenestralis
stapedial muscle fossa
fenestra vestibuli
C
ant.
dor. med.
tegmen tympani
promontorium
ventrolateral tuberosity?
mastoid region
D
dor. med.
dor. lat.
internal acoustic meatus
prefacial commissure
tegmen tympani
promontorium
E
ant.
vent. med.
crista transversa
prefacial commissure
foramen acousticum inferius
tegmen tympani
cochlear aqueduct
subarcuate depression
vestibular aqueduct
foramen acousticum superius
F
ant.
vent. lat.
basicapsular groove
promontorium
mastoid region
1 cm

Figure 4

Endocast of the left bony labyrinth of *Hipparion depereti* (NMB.A.Mo.655) from Montredon.

(A) Anterior view. (B) Posterior view. (C) Lateral view. (D) Dorsal view. *Dor.* = dorsal, *lat.* = lateral, *pos.* = posterior.

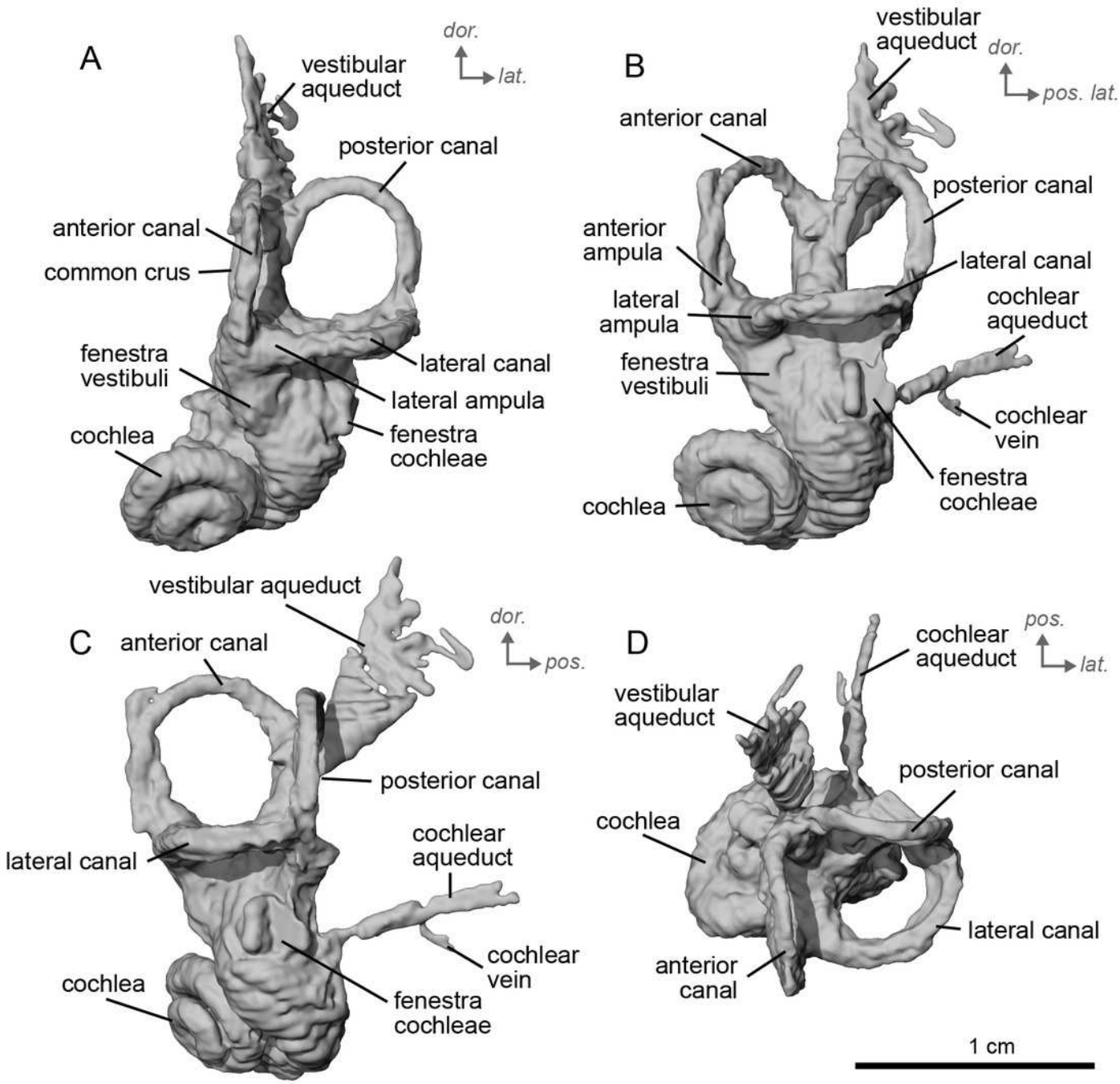
A
dor.
lat.
vestibular aqueduct
posterior canal
anterior canal
common crus
fenestra vestibuli
lateral canal
lateral ampula
cochlea
fenestra cochleae
B
vestibular aqueduct
dor.
pos. lat.
anterior canal
posterior canal
anterior ampula
lateral canal
lateral ampula
cochlear aqueduct
fenestra vestibuli
cochlear vein
fenestra cochleae
cochlea
C
vestibular aqueduct
dor.
pos.
anterior canal
posterior canal
lateral canal
cochlear aqueduct
cochlear vein
cochlea
fenestra cochleae
D
pos.
cochlear aqueduct
lat.
vestibular aqueduct
posterior canal
cochlea
lateral canal
anterior canal
1 cm

Figure 5

Left petrosal (NMB.Ccd.3) of *Hipparion concudense* from Concud3.

(A) Ventrolateral transparent view. (B) Ventrolateral opaque view. (C) dorsolateral view. (D) Anterior view. (E) Dorsomedial view. (F) Ventromedial view. *Ant* = anterior, *dor.* = dorsal, *lat.* = lateral, *med.* = medial, *vent.* = ventral.

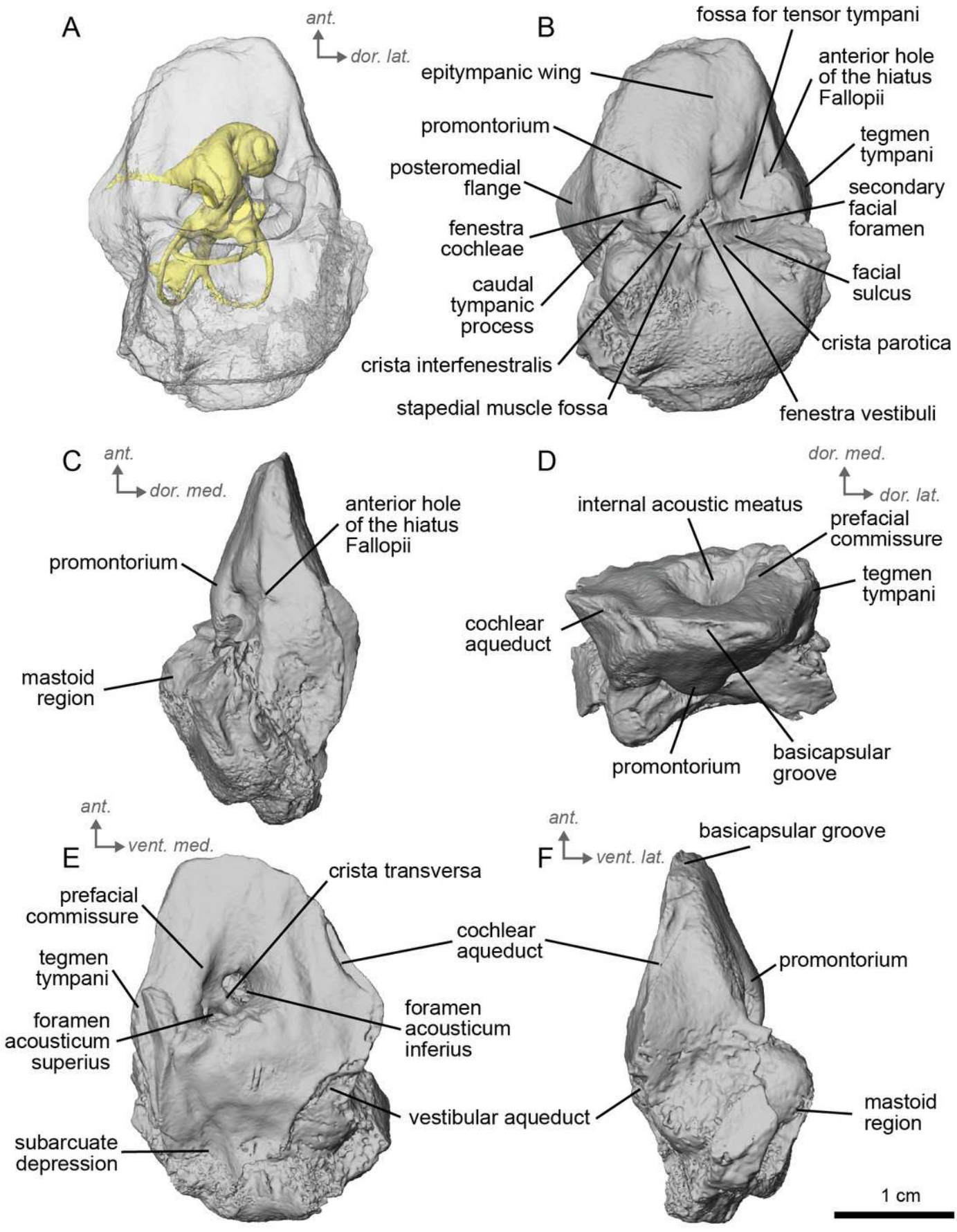
A
ant.
dor. lat.
B
fossa for tensor tympani
epitympanic wing
anterior hole of the hiatus Fallopii
promontorium
tegmen tympani
posteromedial flange
secondary facial foramen
fenestra cochleae
facial sulcus
caudal tympanic process
crista parotica
crista interfenestralis
stapedial muscle fossa
fenestra vestibuli
C
ant.
dor. med.
anterior hole of the hiatus Fallopii
promontorium
mastoid region
D
dor. med.
dor. lat.
internal acoustic meatus
prefacial commissure
tegmen tympani
cochlear aqueduct
promontorium
basicapsular groove
E
ant.
vent. med.
crista transversa
prefacial commissure
cochlear aqueduct
tegmen tympani
foramen acousticum superius
foramen acousticum inferius
vestibular aqueduct
subarcuate depression
F
ant.
vent. lat.
basicapsular groove
promontorium
mastoid region
1 cm

Figure 6

Endocast of the left bony labyrinth of *H. concudense* (NMB.Ccd.3) from Concud3.

(A) Anterior view. (B) Posterior view. (C) Lateral view. (D) Dorsal view. *Dor.* = dorsal, *lat.* = lateral, *pos.* = posterior.

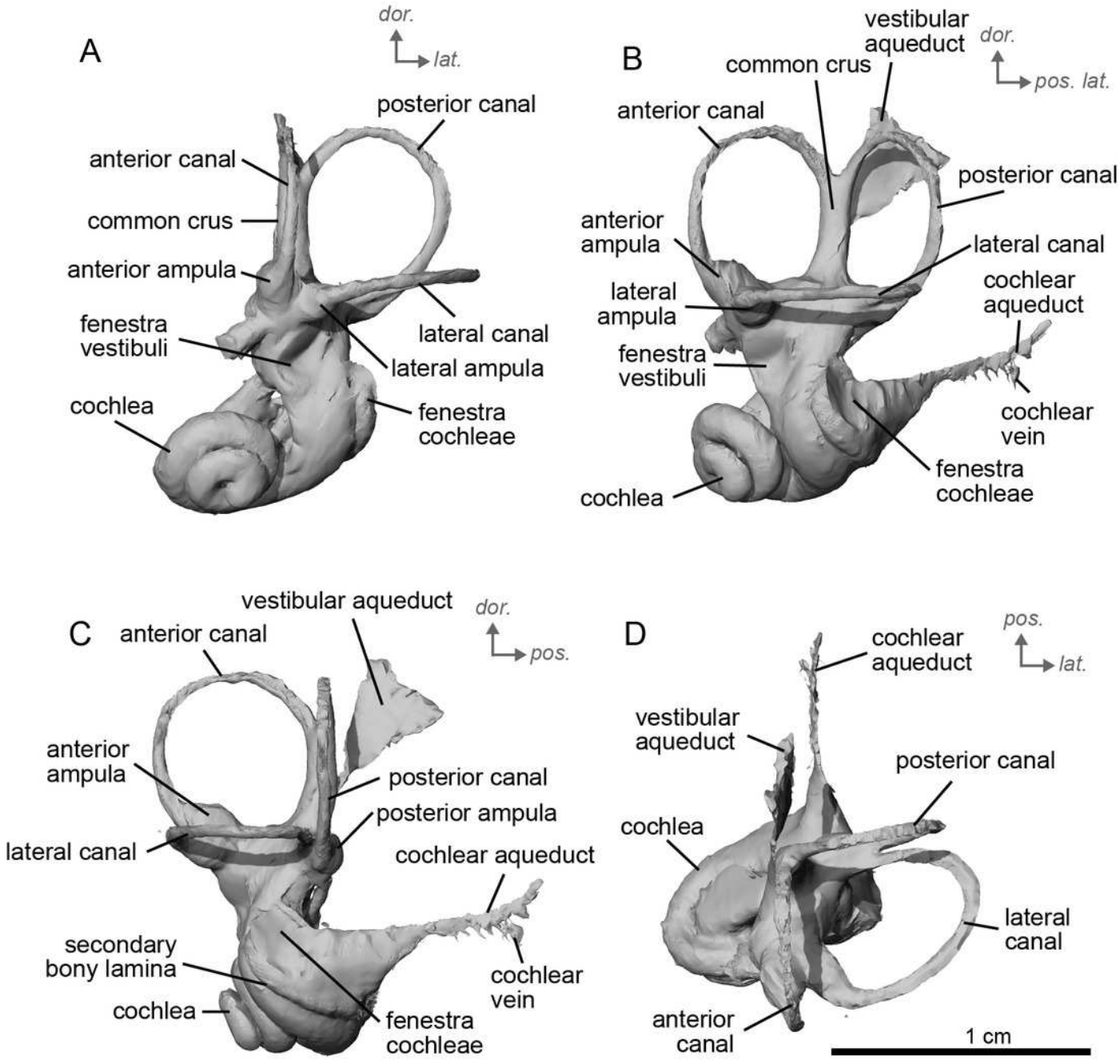

Figure 7

Left stapes preserved within the petrosals of fossil equids.

(A) *Hipparion concudense* (NMB.Ccd.3). (B) *Equus stenonis* (NMB.V.A.2753). (C) *Equus senezensis* (NMB.Se.141). Abbreviations: bs, *basis stapedis*; cas, *crus anterius stapedis*; cps, *crus posterius stapedis* ; fi, *foramen intercrurale*; pms, *processus muscularis stapedis*.

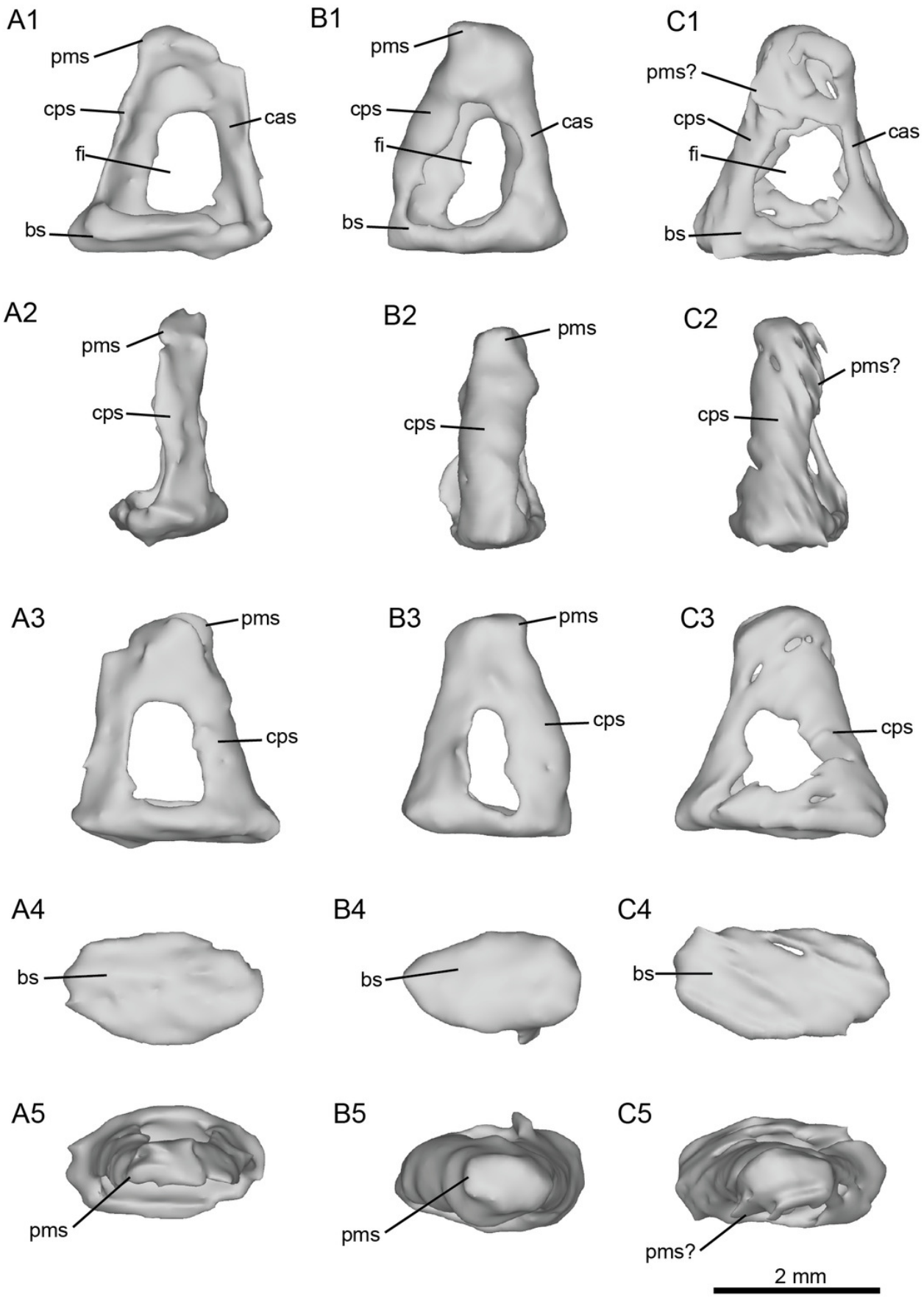
A1
pms
cps
cas
fi
bs
B1
pms
cps
cas
fi
bs
C1
pms?
cps
cas
fi
bs
A2
pms
cps
B2
pms
cps
C2
pms?
cps
A3
pms
cps
B3
pms
cps
C3
cps
A4
bs
B4
bs
C4
bs
A5
pms
B5
pms
C5
pms?
2 mm

Figure 8

Left petrosal (NMB.V.A.2753) of *Equus stenonis* from Valdarno.

(A) Ventrolateral transparent view. (B) Ventrolateral opaque view. (C) dorsolateral view. (D) Anterior view. (E) Dorsomedial view. (F) Ventromedial view. *Ant* = anterior, *dor.* = dorsal, *lat.* = lateral, *med.* = medial, *vent.* = ventral.

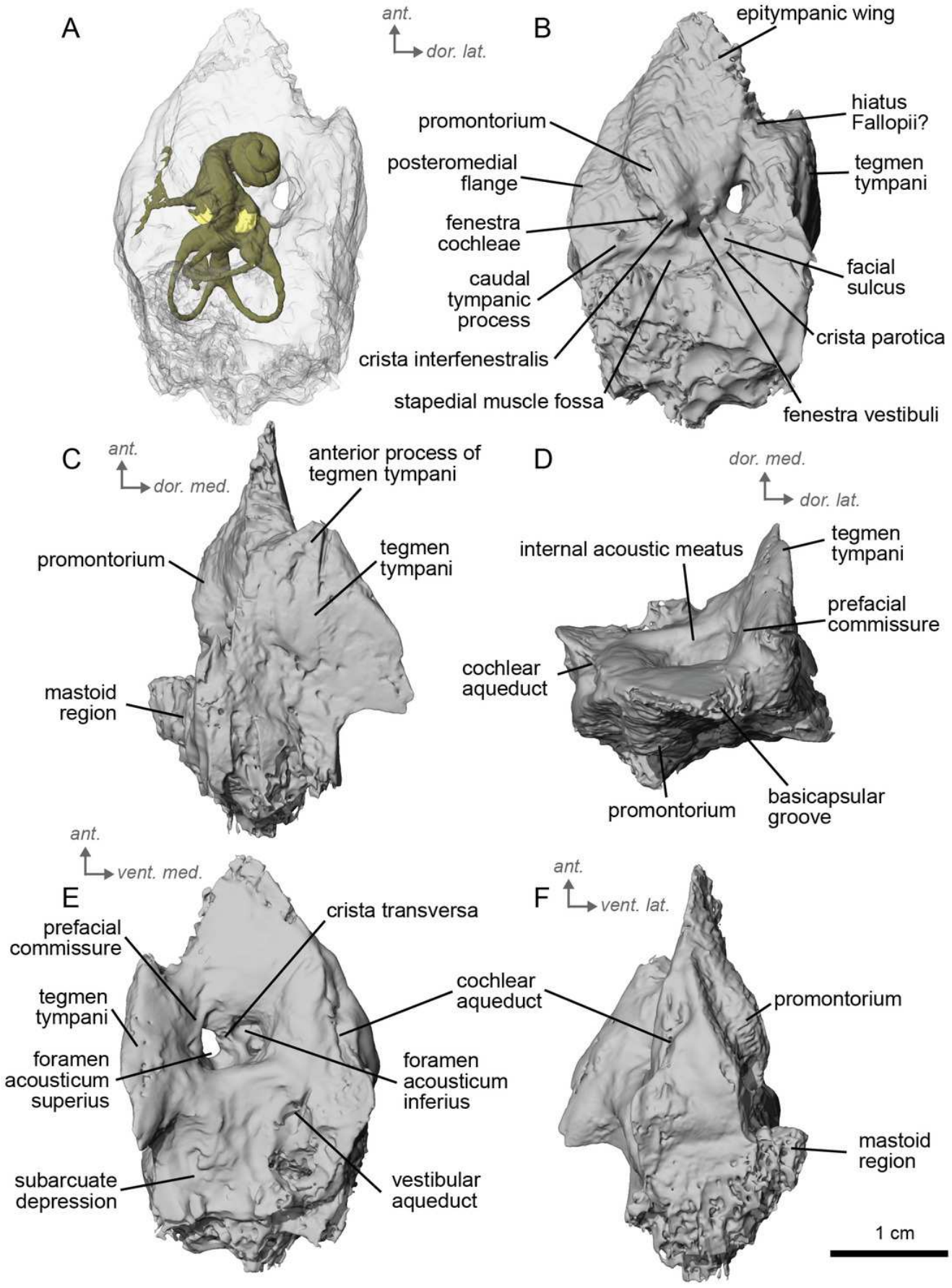
A
ant.
dor. lat.
B
epitympanic wing
hiatus Fallopii?
promontorium
posteromedial flange
tegmen tympani
fenestra cochleae
facial sulcus
caudal tympanic process
crista parotica
crista interfenestralis
stapedial muscle fossa
fenestra vestibuli
C
ant.
dor. med.
anterior process of tegmen tympani
promontorium
tegmen tympani
mastoid region
D
dor. med.
dor. lat.
internal acoustic meatus
tegmen tympani
prefacial commissure
cochlear aqueduct
promontorium
basicapsular groove
E
ant.
vent. med.
crista transversa
prefacial commissure
cochlear aqueduct
tegmen tympani
foramen acousticum superius
foramen acousticum inferius
subarcuate depression
vestibular aqueduct
F
ant.
vent. lat.
cochlear aqueduct
promontorium
mastoid region
1 cm

Figure 9

Endocast of the left bony labyrinth of *E. stenonis* (NMB.V.A.2753) from Valdarno.

(A) Anterior view. (B) Posterior view. (C) Lateral view. (D) Dorsal view. *Dor.* = dorsal, *lat.* = lateral, *pos.* = posterior.

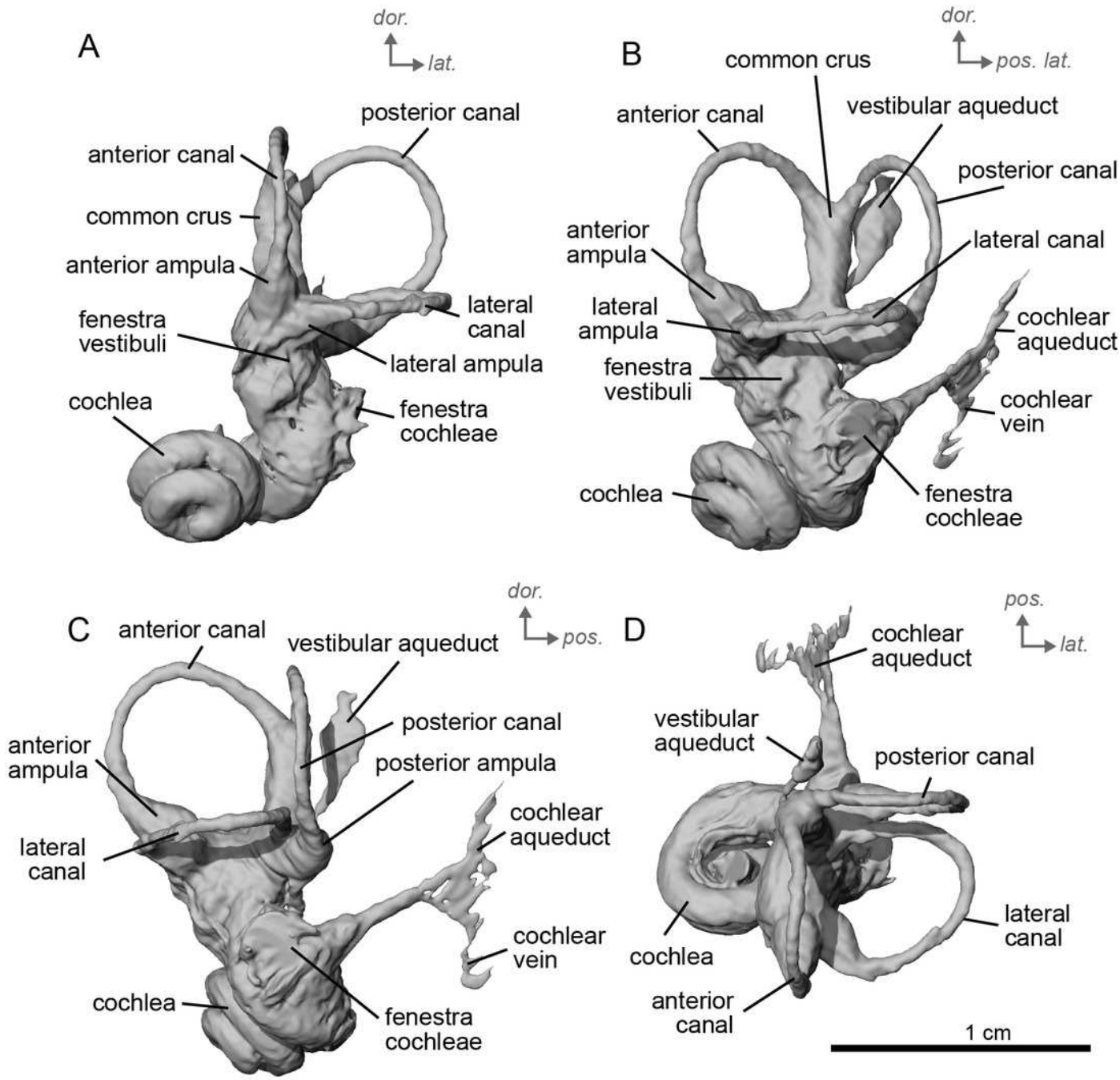
A
dor.
lat.
posterior canal
anterior canal
common crus
anterior ampula
fenestra vestibuli
lateral canal
lateral ampula
cochlea
fenestra cochleae
B
dor.
pos. lat.
common crus
anterior canal
vestibular aqueduct
posterior canal
anterior ampula
lateral canal
lateral ampula
cochlear aqueduct
fenestra vestibuli
cochlear vein
cochlea
fenestra cochleae
C
dor.
pos.
anterior canal
vestibular aqueduct
posterior canal
anterior ampula
posterior ampula
cochlear aqueduct
lateral canal
cochlear vein
cochlea
fenestra cochleae
D
pos.
lat.
cochlear aqueduct
vestibular aqueduct
posterior canal
lateral canal
cochlea
anterior canal
1 cm

Figure 10

Left petrosal (NMB.Se.141) of *Equus senezensis* from Senèze.

(A) Ventrolateral transparent view. (B) Ventrolateral opaque view. (C) dorsolateral view. (D) Anterior view. (E) Dorsomedial view. (F) Ventromedial view. *Ant* = anterior, *dor.* = dorsal, *lat.* = lateral, *med.* = medial, *vent.* = ventral.

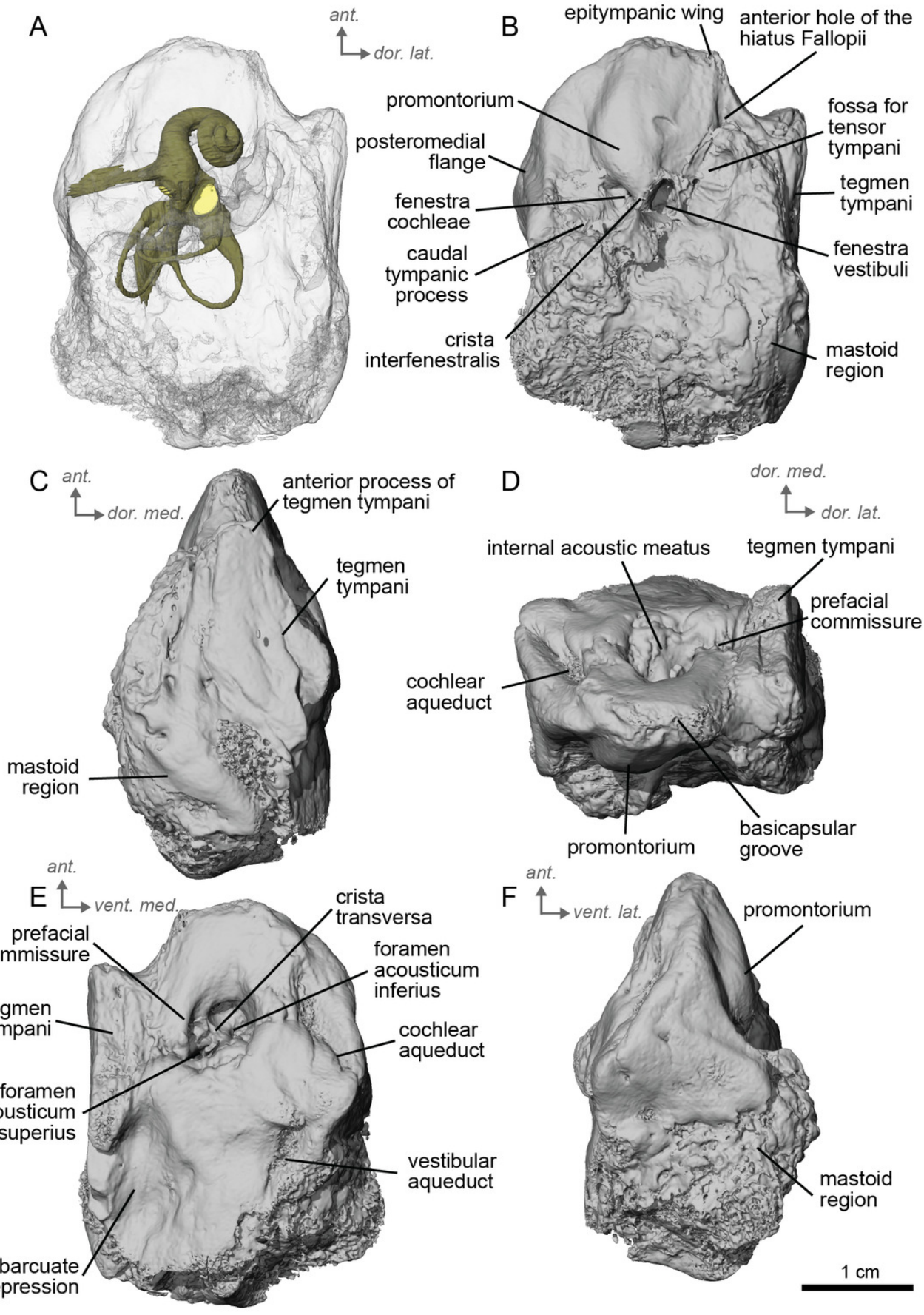
A
ant.
dor. lat.
B
epitympanic wing
anterior hole of the hiatus Fallopii
promontorium
fossa for tensor tympani
posteromedial flange
tegmen tympani
fenestra cochleae
fenestra vestibuli
caudal tympanic process
crista interfenestralis
mastoid region
C
ant.
dor. med.
anterior process of tegmen tympani
tegmen tympani
mastoid region
D
dor. med.
dor. lat.
internal acoustic meatus
tegmen tympani
prefacial commissure
cochlear aqueduct
promontorium
basicapsular groove
E
ant.
vent. med.
crista transversa
prefacial commissure
foramen acousticum inferius
tegmen tympani
cochlear aqueduct
foramen acousticum superius
vestibular aqueduct
subarcuate depression
F
ant.
vent. lat.
promontorium
mastoid region
1 cm

Figure 11

Right petrosal (NMB.Se.554) of *Equus senezensis* from Senèze (mirrored).

(A) Ventrolateral transparent view. (B) Ventrolateral opaque view. (C) dorsolateral view. (D) Anterior view. (E) Dorsomedial view. (F) Ventromedial view. *Ant* = anterior, *dor.* = dorsal, *lat.* = lateral, *med.* = medial, *vent.* = ventral.

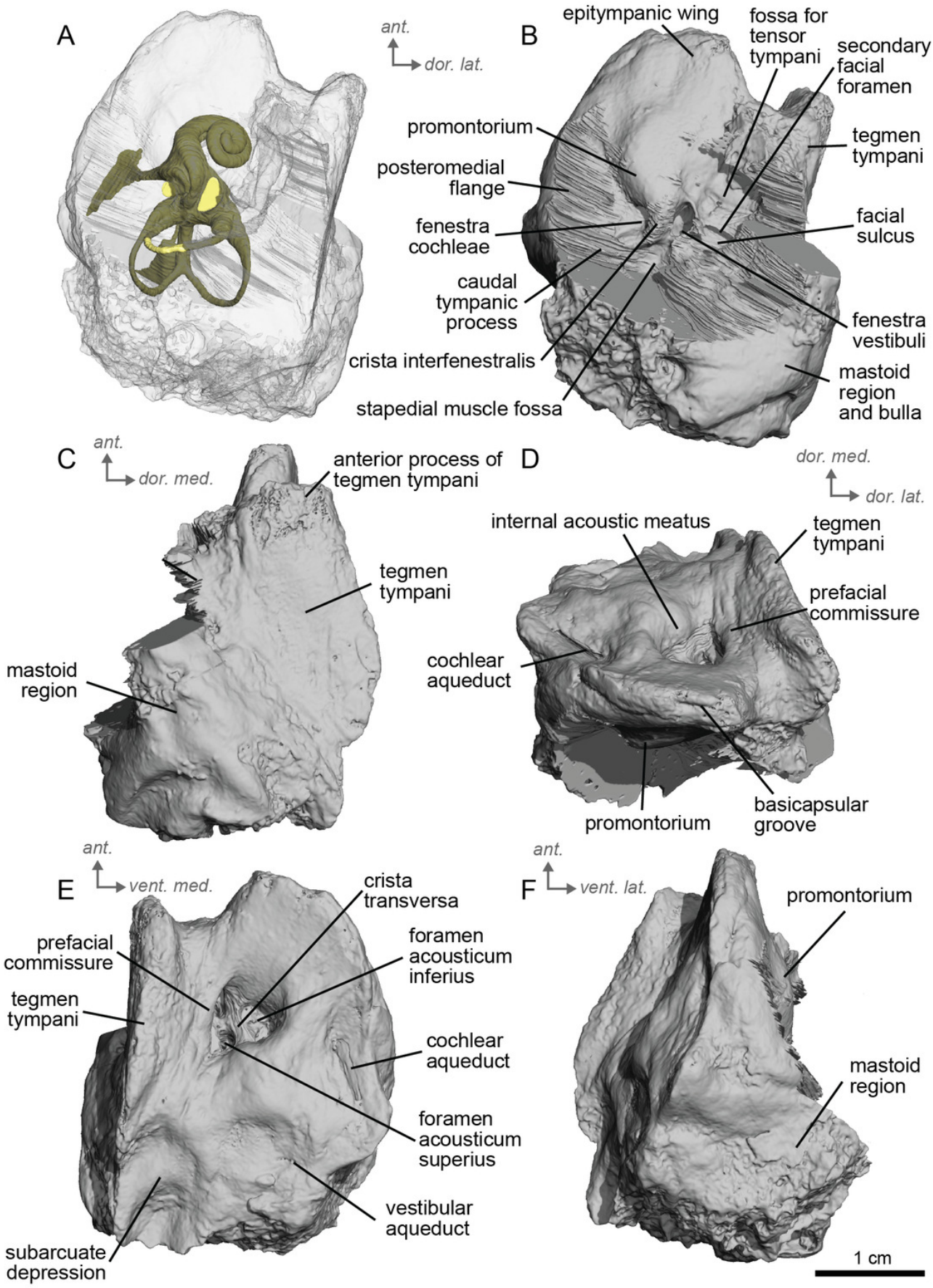
A
ant.
dor. lat.
B
epitympanic wing
fossa for tensor tympani
secondary facial foramen
promontorium
tegmen tympani
posteromedial flange
fenestra cochleae
facial sulcus
caudal tympanic process
fenestra vestibuli
crista interfenestralis
mastoid region and bulla
stapedial muscle fossa
C
ant.
dor. med.
anterior process of tegmen tympani
tegmen tympani
mastoid region
D
dor. med.
dor. lat.
internal acoustic meatus
tegmen tympani
prefacial commissure
cochlear aqueduct
promontorium
basicapsular groove
E
ant.
vent. med.
crista transversa
prefacial commissure
foramen acousticum inferius
tegmen tympani
cochlear aqueduct
foramen acousticum superius
vestibular aqueduct
subarcuate depression
F
ant.
vent. lat.
promontorium
mastoid region
1 cm

Figure 12

Endocast of the left bony labyrinth of *Equus senezensis* (NMB.Se.141) from Senèze.

(A) Anterior view. (B) Posterior view. (C) Lateral view. (D) Dorsal view. *Dor.* = dorsal, *lat.* = lateral, *pos.* = posterior.

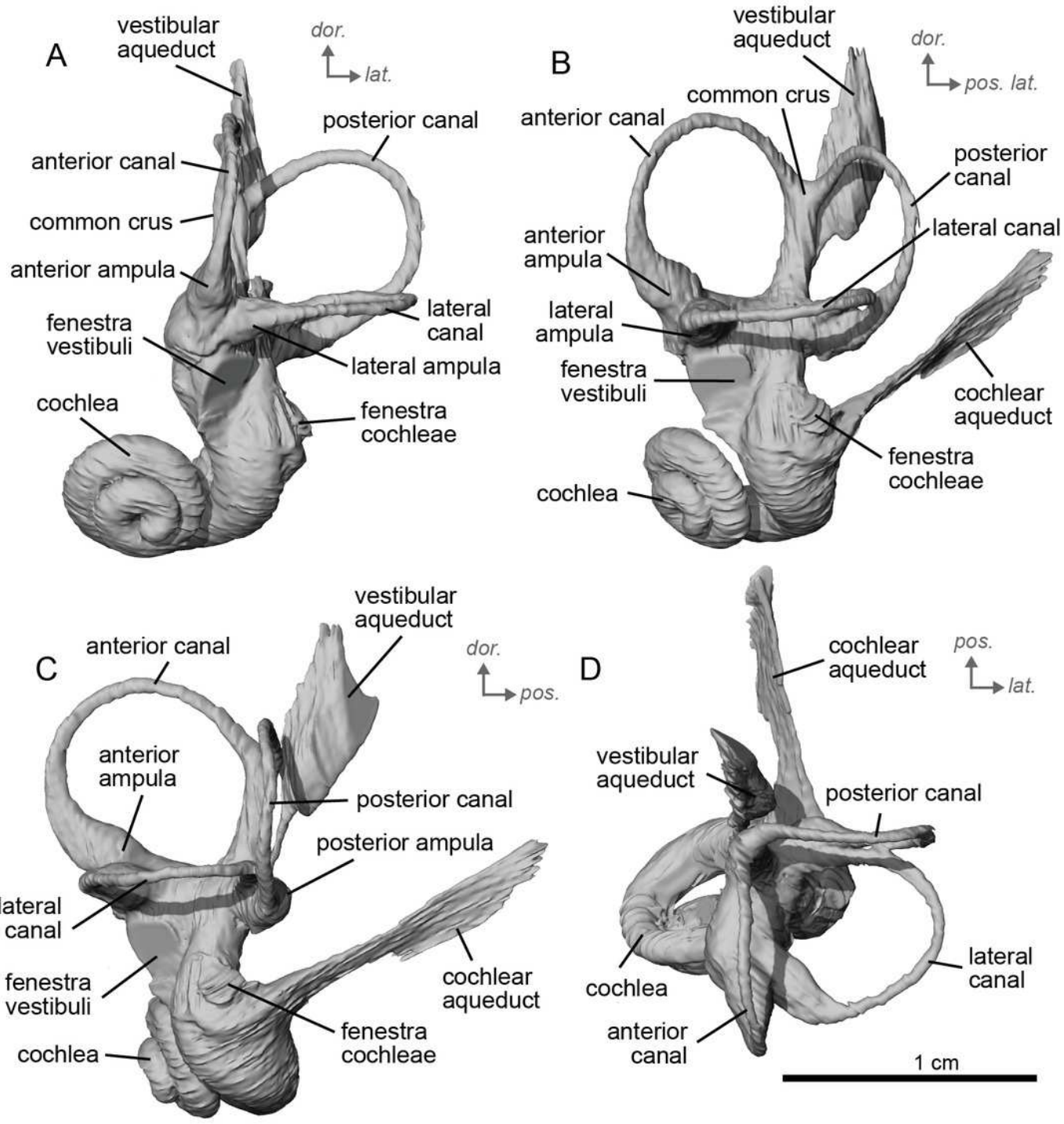
A
vestibular aqueduct
dor.
lat.
posterior canal
anterior canal
common crus
anterior ampula
lateral canal
fenestra vestibuli
lateral ampula
cochlea
fenestra cochleae
B
vestibular aqueduct
dor.
pos. lat.
common crus
anterior canal
posterior canal
lateral canal
anterior ampula
lateral ampula
fenestra vestibuli
cochlear aqueduct
fenestra cochleae
cochlea
C
vestibular aqueduct
anterior canal
dor.
pos.
anterior ampula
posterior canal
posterior ampula
lateral canal
cochlear aqueduct
fenestra vestibuli
fenestra cochleae
cochlea
D
cochlear aqueduct
pos.
lat.
vestibular aqueduct
posterior canal
lateral canal
cochlea
anterior canal
1 cm

Figure 13

Endocast of the right bony labyrinth of *Equus senezensis* (NMB.Se.554) from Senèze (mirrored).

(A) Anterior view. (B) Posterior view. (C) Lateral view. (D) Dorsal view. *Dor.* = dorsal, *lat.* = lateral, *pos.* = posterior.

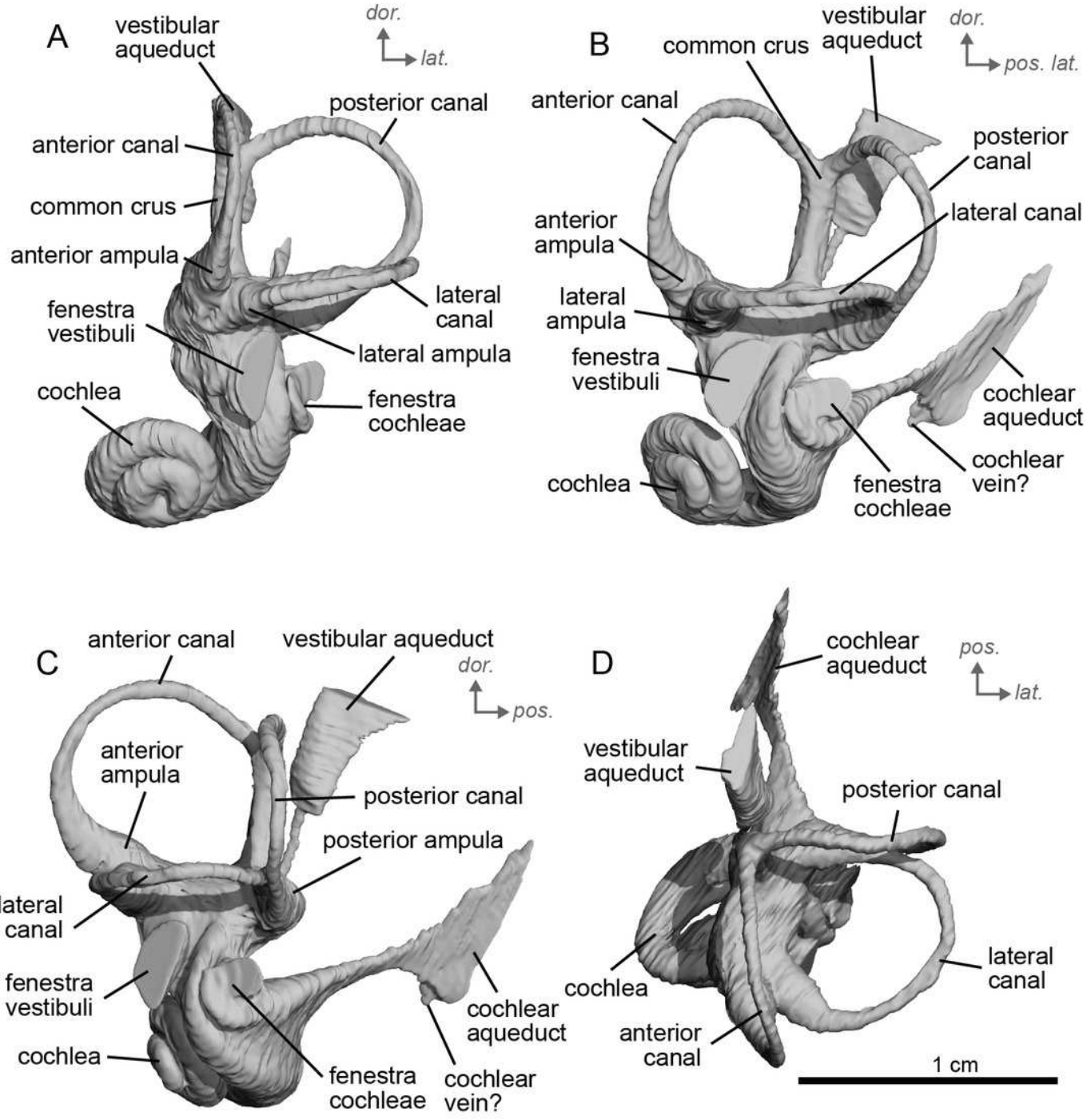
A
vestibular aqueduct
dor.
lat.
posterior canal
anterior canal
common crus
anterior ampula
lateral canal
fenestra vestibuli
lateral ampula
cochlea
fenestra cochleae
B
common crus
vestibular aqueduct
dor.
pos. lat.
anterior canal
posterior canal
lateral canal
anterior ampula
lateral ampula
fenestra vestibuli
cochlear aqueduct
cochlear vein?
cochlea
fenestra cochleae
C
anterior canal
vestibular aqueduct
dor.
pos.
anterior ampula
posterior canal
posterior ampula
lateral canal
fenestra vestibuli
cochlear aqueduct
cochlea
fenestra cochleae
cochlear vein?
D
cochlear aqueduct
pos.
lat.
vestibular aqueduct
posterior canal
lateral canal
cochlea
anterior canal
1 cm

Figure 14

Phylogeny of the studied Equidae based on ear region characters.

Strict consensus tree of 11 trees of 24 steps (CI=0.88, HI=0.13, RI=0.80) with *Hyopsodus* used as outgroup, obtained by an exhaustive search with a parsimony algorithm in PAUP*4. Non-ambiguous apomorphies are indicated as “character number:state” at nodes. Bootstrap support values above 50 are reported in bold font below nodes. Silhouettes of horses from Phylopic made by Julian Bayona.

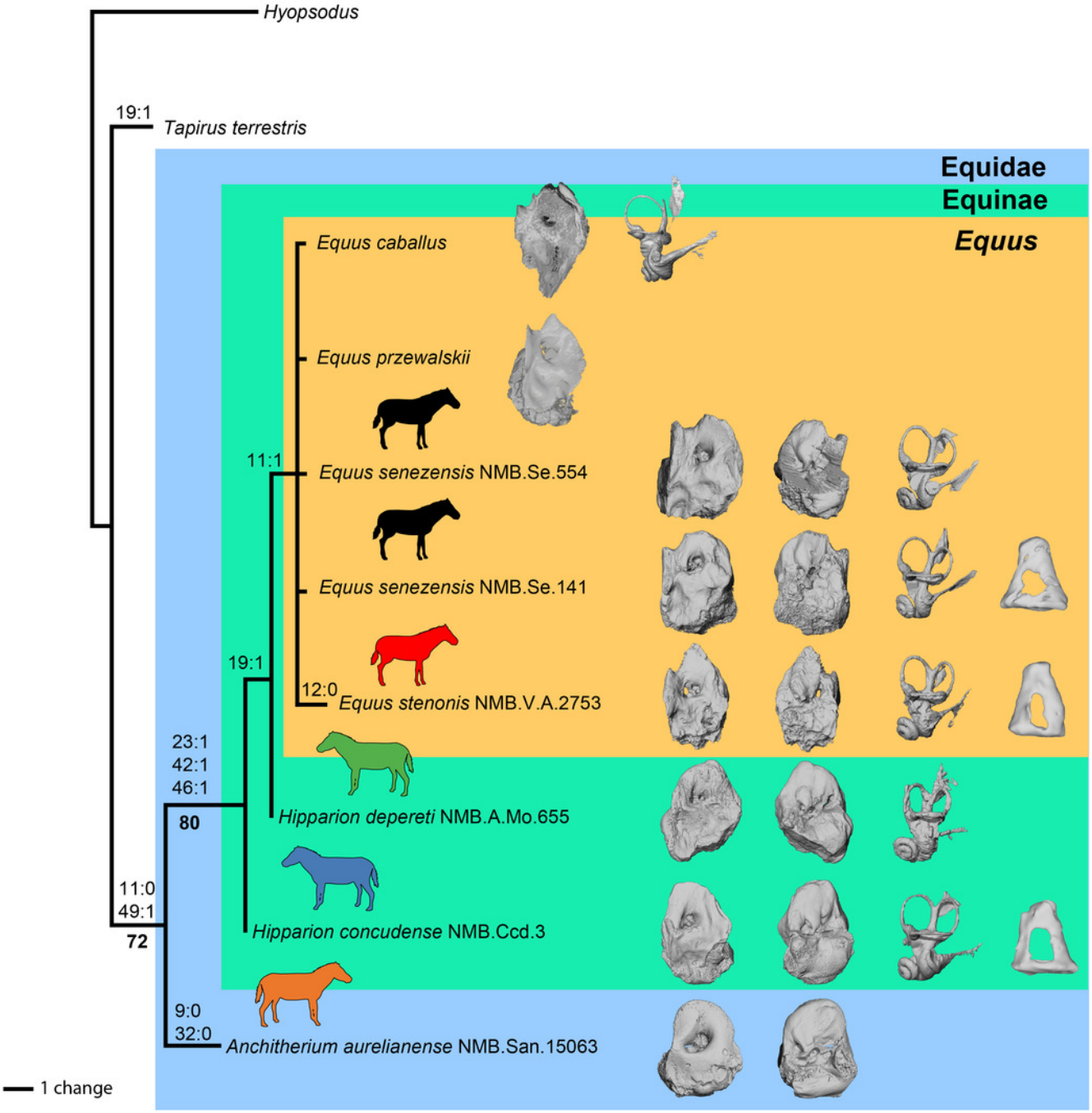
Hyopsodus
19:1
Tapirus terrestris
Equidae
Equinae
Equus
Equus caballus
Equus przewalskii
11:1
Equus senezensis NMB.Se.554
Equus senezensis NMB.Se.141
19:1
12:0
Equus stenonis NMB.V.A.2753
23:1
42:1
46:1
80
Hipparion depereti NMB.A.Mo.655
11:0
49:1
72
Hipparion concudense NMB.Ccd.3
9:0
32:0
Anchitherium aurelianense NMB.San.15063
1 change